Accurate modeling of the dynamics of dissociative chemisorption on metal surfaces

Gerrits, N.

Chapter 5

When Does GGA-DFT Get Molecule-Metal Surface Reaction Barriers Right, and What to Do if it Doesn't

This chapter is based on Gerrits, N.; Smeets, E. W. F.; Vuckovic, S.; Powell, A. D.; Doblhoff-Dier, K.; Kroes, G.-J. Density Functional Theory for Molecule–Metal Surface Reactions: When Does the Generalized Gradient Approximation Get It Right, and What to Do If It Does Not. *J. Phys. Chem. Lett.* **2020**, *11*, 10552–10560, DOI: 10.1021/acs.jpclett.0c02452

Abstract

While density functional theory (DFT) is perhaps the most used electronic structure theory in chemistry, many of its practical aspects remain poorly understood. For instance, DFT at the generalized gradient approximation (GGA) level tends to fail miserably at describing gas phase reaction barriers, while it performs surprisingly well for many molecule-metal surface reactions. GGA-DFT also fails for many systems in the latter category, and up to now it has not been clear when one may expect it to work. This chapter shows that GGA-DFT tends to work if the difference between the work function of the metal and the molecule's electron affinity is greater than ≈7 eV, and to fail if this difference is smaller, with sticking of O_2 on Al(111) being a spectacular example. Using dynamics calculations it is shown that, for this system, the DFT problem may be solved as done for gas phase reactions, i.e., by resorting to hybrid functionals, but using screening at long range to obtain a correct description of the metal. The results suggest the GGA error in the O_2 + Al(111) barrier height to be functional driven. The results also suggest the possibility to compute potential energy surfaces for the difficult-to-treat systems with

computationally cheap non-self-consistent calculations in which a hybrid functional is applied to a GGA density.

5.1 Introduction

Kohn-Sham DFT has become very popular and is now being used in more than 30 000 papers per year[1]. Nevertheless, much of the theory remains not yet well understood, even concerning much of its practical aspects. One surprising practical aspect is that density functionals (DFs) at the generalized gradient approximation (GGA) level are quite accurate for barriers for dissociative chemisorption (DC) reactions on metal surfaces. In contrast, semi-local functionals tend to systematically underestimate reaction barrier heights of gas phase reactions[2, 3], and it has been assumed that this overestimation should carry over to surface reactions in general[4]. Nonetheless, a semi-empirical version of DFT, the specific reaction parameter (SRP) approach to DFT, has achieved chemically accurate descriptions of sticking in many molecule-metal surface systems by using functionals in which the exchange part is a weighted average of GGA exchange functionals[5–13]. Here, often (the exchange part of) the PBE[14] (or PW91[15]) and the RPBE[16] DFs are used, with PBE and PW91 often yielding too low, and RPBE often too high barriers[5, 7]. Dynamics studies using non-empirical GGA DFs have semi-quantitatively described many experiments on DC on metals[17–21]. Perhaps even more surprisingly a recent comparison of DFT results for a database of molecule-metal surface reactions based on experiments and SRP-DFT (SBH10) suggested a better performance for a GGA-exchange based DF (i.e., BEEF-vdW[22]) than for the meta-GGA and screened hybrid representative examples that were tested[23].

In spite of the above, also many molecule-metal surface systems exist for which SRP-DFs based on GGA exchange DFs do not work. By this we mean that even the most repulsive GGA exchange DFs still obeying the uniform electron gas limit (such as RPBE, a non-empirical functional which describes adsorption on metals with quite high accuracy, but already performs rather poorly at describing solid state properties[22, 24]) are too reactive compared to experiment, even when simulating the effect of energy dissipation to electron-hole pairs and surface phonons[25–30]. As a result, the barrier height cannot be "tweaked" to a good value by mixing exchange DFs yielding too high barriers (such as RPBE) and too low barriers (as often the case with PBE or PW91). That is a pity, as a DC transition state (TS) on a metal surface is often the rate-controlling state in industrially important heterogeneously catalyzed processes[31–33] like ammonia production[34] and steam reforming[35]. A

further problem is that it is not clear which property of the system determines whether GGA-DFT may yield a reliable barrier height. Reasons to explain the GGA-DFT failure for individual systems have, however, been cited, with an often cited reason being that electron transfer occurs from the metal surface to the molecule[36, 37].

In this connection often reference is made to the following explanation for why GGA-DFT fails at describing gas phase reactions: the GGA's tendency to underestimate gas phase barrier heights is caused by the electrons delocalizing over additional atoms at the TS, artificially lowering the GGA energy of the TS relative to that of the reactants[3, 38, 39]. The delocalization error finds its origin in what has been called "the lack of derivative discontinuities of semi-local functionals" or alternatively the violation of the Perdew-Parr-Levy-Balduz condition[40] by these functionals. According to Yang and co-workers[41] the delocalization error is similar, but not equal to the self-interaction error (SIE)[42], which is also often invoked to explain the underestimation of gas phase reaction barrier heights. However, the above does not yet explain why GGA-DFT *does* work for many molecule-metal surface reactions. Also, a property of the system on the basis of which one could straightforwardly predict whether GGA-DFT should, at least in principle, work is still missing. Fortunately, the "charge transfer" explanation does suggest such a criterion, as will be shown here.

This chapter shows that a single, albeit composite, property of molecule-metal surface systems exists on the basis of which one can decide whether it should be possible to find a GGA functional with which one can describe the barrier to dissociative chemisorption with chemical accuracy. This allows one to define a single corresponding criterion stating whether GGA functionals should be able to deliver chemical accuracy for the corresponding "easy-to-handle" reactions. Also, the solution applicable to the problem that gas phase reaction barriers are not well-described with GGA functionals (i.e., resorting to hybrid functionals) also works for a prominent example of "difficult" surface reactions, i.e., that of O_2 + Al(111). These findings suggest the possibility of extending SRP-DFT to the full range of dissociative chemisorption reactions on metals. Such an extension should enable the development of databases for such reactions[43] without bias to specific rungs of functionals, similar to databases that already exist for gas phase reactions[2, 3].

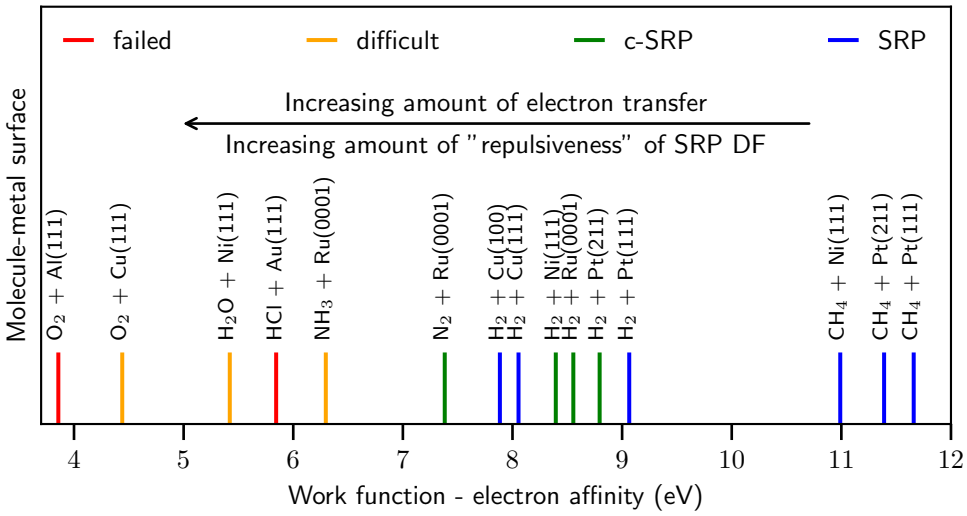

FIGURE 5.1: Correlation between the difference of the work function of the metal surface and the electron affinity of the molecule (eV) with the ability of GGA exchange-based DFs to accurately describe barrier heights to DC in the systems described. Red, orange, green and blue indicate whether efforts to develop an SRP DF based on GGA exchange for a molecule-metal surface reaction have failed, proven difficult, yielded a candidate SRP (c-SRP) DF, or yielded an SRP DF, respectively. The values of the work functions (Table 5.A.1) and electron affinities (Table 5.A.2) are obtained as described in Section 5.A.2.

5.2 Analysis of Previous Results

Obviously, one would expect the tendency of a system to display charge transfer to correlate with the difference $(W - E_{ea})$ between the work function W of the metal and the electron affinity E_{ea} of the molecule. Systematic evidence is collected in Figure 5.1, where it is shown how the ability to accurately describe the measured reactivity of molecule-metal surface systems with DFs containing GGA exchange correlates with $(W - E_{ea})$. Figure 5.1 shows that it has been possible to achieve chemical accuracy in descriptions of sticking experiments with GGA-exchange based SRP-DFs[5, 6, 8–10] (in blue) and candidate SRP-DFs[7, 11–13] (in green) if $(W - E_{ea})$ exceeds 7 eV. (Candidate SRP-DFs usually describe a sticking experiment on a specific system with chemical accuracy, but their validity has not (yet) been confirmed through comparison with another experiment on the same system[7, 12, 13].) However, for systems with $(W - E_{ea}) < 7$ eV DFs with repulsive RPBE exchange either overestimate sticking notoriously [25, 26, 29, 44–46] (red), or they show a suspect performance[27, 28, 30, 47] (orange). In Figure 5.1 a trend is also observed that when the difference between W and E_{ea} decreases, so that one might also expect the amount of electron transfer to increase, the SRP or GGA DF needs to be made increasingly repulsive to describe the system's reactivity with chemical accuracy. For example, CH_4 + Ni(111)[48] and Pt(111)[49] are quite well-described with the attractive PBE functional[14], and this is also true for H_2 + Pt(111)[50] (here the PW91[15] functional was used, which may be considered the predecessor to PBE, which was designed to replace it[14]) and Ru(0001)[7]. On the other hand, the SRP DF for H_2 + Cu(111)[5] and Cu(100)[6] needs to contain about 50% RPBE exchange, and a good description of N_2 + Ru(0001) was recently obtained with the RPBE DF[11].

A caveat with the above comparison between dynamics based on DFT and experiment is that the difference $(W - E_{ea})$ has also been correlated with the extent to which (reactive) scattering in a system may be affected by energy dissipation through electron-hole pair excitation[51]. Here, the reasoning used could be that (electronically adiabatic) dynamics simulations using repulsive RPBE exchange might overestimate the DC probability because the dissipation of the molecule's incident kinetic energy to electron-hole pairs is not modeled. However, in this type of analysis evidence for strongly nonadiabatic molecule-metal surface scattering comes mostly from experiments on vibrationally inelastic scattering[52, 53] and scattering of H-atoms from metal surfaces[54], whereas dynamics calculations only suggested small effects of electron-hole pair excitation in some of the hard-to-model systems in Figure 5.1, i.e., D_2O + Ni(111)[55] and HCl + Au(111)[29]. More definite evidence

TABLE 5.1: Barrier heights (in kJ/mol) computed with DMC are compared with values calculated with the RPBE and PBE (or PW91‡) DFs of DFT for three different H_2 + metal surface systems. Also shown are the differences ($W - E_{ea}$, in eV) between the work function of the metal, and the electron affinity of H_2 as computed at the semi-empirical composite G4 level of theory[60]. The values for Mg(0001) are calculated with PBE-DFT[a][61] or measured for a thin layer of Mg[b][62].

Molecule-metal surface	E_b^{DMC}	E_b^{RPBE}	E_b^{PBE}	$W - E_{ea}$
H_2 + Cu(111)	54.4 ± 4.2[57]	79.1[5]	46.9‡[5]	8.06
H_2 + Al(110)	105.0 ± 0.8[58]	100.4[58]	79.9[58]	7.39
H_2 + Mg(0001)	113.8 ± 2.9[59]	103.3[59]	84.9[59]	6.92[a], 6.82[b]

that electronically nonadiabatic effects are most likely not the explanation for the trend observed in Figure 5.1 comes from a direct comparison between barrier heights obtained with first-principles and RPBE calculations. Barrier heights obtained with diffusion Monte Carlo (DMC)[56] and DFT using the RPBE and PBE DFs are compared for three H_2 + metal surface systems in Table 5.1. For H_2 + Cu(111)[57] and Al(110)[58] GGA DFT is able to reproduce the DMC barrier height, and $(W - E_{ea}) > 7\,\text{eV}$. In contrast, the RPBE DF underestimates the DMC barrier height for H_2 + Mg(0001)[59] ($W - E_{ea} < 7\,\text{eV}$). Note that for H_2 + Cu(111) DMC was shown[57] to be able to reproduce the best estimate of the barrier height to within $(6.7 \pm 4.2)\,\text{kJ/mol}$. Below an explanation is attempted of the success of exchange-correlation functionals containing semi-local exchange at describing reaction barrier heights for molecule-metal surface systems with $(W - E_{ea}) > 7\,\text{eV}$ and of their failure for systems with $(W - E_{ea}) < 7\,\text{eV}$. However, first we investigate whether and how the problem can be fixed for one of the "difficult" systems decribed above.

The standard way of dealing with errors in barriers for gas phase reactions is to ascend the DFT ladder to higher level functionals, i.e., to use meta-GGA or hybrid DFs[2, 3]. As will be shown now, this route can also be successful when dealing with molecule-metal surface reactions. One clear example where DFT tends to overestimate the reactivity is for useful benchmark systems[43] of activated dissociation of O_2 on metal surfaces[25, 27] (see also the SI), with O_2 + Al(111) being an infamous example[25]. Molecular dynamics (MD) simulations employing GGA DFs predict a non-activated reaction[25, 44], whereas experiments show that the reaction is activated[63, 65] (see Figure 5.2a). So far, of the MD simulations that use a GGA DF (or a semi-empirical potential energy surface (PES) based on a GGA DF)[25, 44, 66] only calculations that

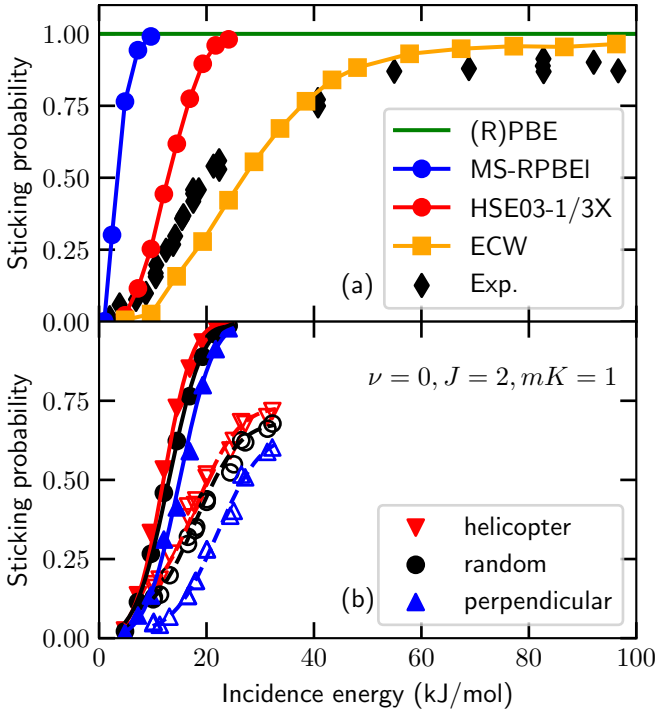

FIGURE 5.2: (a) Sticking probability of O_2 on Al(111) as a function of translational energy for normal incidence. The green line indicates results obtained with the (R)PBE DF[25, 44], whereas the blue and red circles indicate QCT results obtained here with the MS-RPBEl and HSE03-1/3X DFs, respectively. The black diamonds and orange squares indicate experimental results[63] and QCT results obtained with an ECW PES[64], respectively. (b) Sticking probability of O_2 ($\nu = 0, J = 2, K = 1$) on Al(111) for the helicopter (red downward pointing triangle), random (black circle), and perpendicular (blue upward pointing triangle) alignments of the molecule relative to the surface. The solid and open symbols indicate the computed (HSE03-1/3X) and the experimental[65] results, respectively. The lines merely guide the eye.

treat the O_2-metal system nonadiabatically have been shown to yield sticking probabilities in semi-quantitative agreement with experiment. On the other hand, electronically adiabatic simulations that use embedded correlated wave function (ECW) theory for the PES have also yielded quite good agreement with experiment[64] (see Figure 5.2a). The latter results led Carter and co-workers to suggest that modeling electronically nonadiabatic effects should not be necessary for O_2 + Al(111)[37]. Specifically, electronic structure calculations based not only on ECW theory but also on hybrid DFT yield adiabatic barriers[37, 67–72], suggesting that an electronically adiabatic approach could well be valid, but that the way the electronic structure is treated is crucial. However, drawbacks of the ECW method are that it is expensive to use and that it is hard to converge the molecule-surface interaction energy with respect to the size of the embedded cluster[37]. Consequently, Yin et al.[64] had to base their PES on a limited amount of points, which forced them to adopt a fitting method that is of only medium accuracy (i.e., a flexible periodic London-Eyring-Polanyi-Sato (FPLEPS) function[73]) to represent their ECW data. Additionally, it is not so clear how the ECW method could be used in an SRP approach, whereas this is rather obvious for DFT.

5.3 Method

Here, the dissociative chemisorption of O_2 is investigated on a static Al(111) surface with the quasi-classical trajectory (QCT)[74] method using PESs based on DFs that go beyond the standard GGA. Like Carter and co-workers, the static surface approximation and the Born-Oppenheimer approximation is made, thereby neglecting non-adiabatic effects related to the spin- and charge-states of O_2 and to electron-hole pair excitation. For the calculations, 6D PESs have been developed with the meta-GGA MS-RPBEl DF[75] and the screened hybrid HSE03-1/3X DF[76, 77]. The MS-RPBEl DF[75] is able to describe both covalent and metallic interactions accurately by relying on a switching function dependent on the kinetic energy density[78]. In principle, with this DF the SIE is reduced by ensuring that the exact energy of the free hydrogen atom is reproduced. For the metallic density regime the low-order gradient expansion of the exchange energy of the homogeneous electron gas is reproduced, which ensures a good description of the metal. The HSE03-1/3X DF is based on the HSE03 DF[76, 77], with the only difference being the maximum fraction of exact exchange α_X, which may be viewed as a semi-empirical parameter. Specifically, $\alpha_X = 1/3$ is used instead of $\alpha_X = 1/4$, since Cortona and coworkers[79, 80] have shown that increasing α_X to 1/3 is also

valid according to the standard DFT adiabatic connection[79], and that the increase from 1/4 as in PBE0 to 1/3 improves the description of gas phase reaction barriers[80]. More generally, it is known that hybrid functionals with high fractions of exact exchange tend to perform better at describing reaction barrier heights[3, 81–83]. Importantly, the HSE03 DF uses screened exact exchange so that a correct description of the long-range Coulomb interaction is recovered for the metal, and screened hybrid DFT is an order of magnitude cheaper than global hybrid DFT for metals[84–89].

For the MS-RPBEl (HSE03-1/3X) DF a 2×2 Al supercell with 4 layers and 15 (10) Å vacuum distance is used. Furthermore, a plane wave kinetic energy cutoff of 600 (400) eV and an $8 \times 8 \times 1$ Γ-centered k-point grid are used. All DFT calculations are performed with the Vienna Ab-initio Simulation Package (VASP version 5.4.4)[90–94], with a user modification to allow the use of the MS-RPBEl DF, using spin polarization when necessary. The core electrons have been represented with the projector augmented wave (PAW) method[94, 95]. In order to speed up convergence, first-order Methfessel-Paxton smearing[96] with a width parameter of 0.2 eV has been employed. Additional information is provided in the appendix to this chapter.

The slabs are constructed with the ideal DFT lattice constants obtained for the tested functionals (4.045 and 4.022 Å for the MS-RPBEl and HSE03-1/3X DFs, respectively), which have been obtained from bulk calculations. The computed bulk lattice constants are in good agreement with the experimental value of 4.032 Å[97]. Furthermore, all interlayer distances have been optimized, yielding an outer layer expansion of 1.4% for the HSE03-1/3X DF and 1.1% for the MS-RPBEl DF, which is in reasonable agreement with the experimental value of 2.2%[98]. Calculations employing the HSE03-1/3X DF are started from converged spin polarized calculations employing the RPBE DF and then iterated until convergence. Using 2 octa-core Intel E5-2630v3 cpus (i.e., a total of 16 cores), single-point calculations for the O_2 + Al(111) PES take 2 - 6 hours or 1.5 - 5 days for the MS-RPBEl and HSE03-1/3X DFs, respectively. Non-self-consistent single-point calculations employing the HSE03-1/3X DF on the self-consistent electron density yielded by RPBE take 1 - 2 hours.

The PESs are constructed with the CRP[99] (see Section 2.3.1) with the same set-up of geometries sampled as in Ref. [7], except that the r_{O_2} and Z_{O_2} grids are non-equidistant in order to increase the accuracy near the barrier. For the MS-RPBEl DF r_{O_2} =[0.9, 1.0, 1.1, 1.15, 1.2, 1.225, 1.25, 1.275, 1.3, 1.35, 1.4, 1.5, 1.6, 1.7, 1.8] Å and Z_{O_2} =[0.25, 0.75, 1.00, 1.25, 1.50, 1.75, 2.0, 2.25, 2.50, 2.75, 3.00, 3.25, 3.50, 4.00, 4.50] Å are employed. Likewise, for the HSE03-1/3X DF r_{O_2} =[1.0, 1.1, 1.15, 1.175, 1.2, 1.225, 1.25, 1.3, 1.4, 1.5, 1.6] Å and Z_{O_2} =[1.00, 1.50, 2.00, 2.25, 2.50, 2.75, 3.00, 3.25, 3.50] Å are employed. It is checked that

the maximum value of r_{O_2} used is large enough for an accurate evaluation of the sticking probability (S_0, see also below). Furthermore, the atomic 3D PES for the HSE03-1/3X DF is taken from the MS-RPBEl DF, i.e., it is computed with the MS-RPBEl DF instead of the HSE03-1/3X DF. This does not affect the accuracy of the interpolation as the 3D potential is merely to ensure an accurate fit of the PES (i.e., to ensure that the corrugation of the resulting 6D interpolation function is low), and therefore results should not be affected by the choice of the 3D potential as long as it is physically reasonable.

For the MD, the QCT method[74, 100] is employed (see Section 2.2). The sticking probabilities are computed as described in the SI of Ref [64]. A sufficient number of trajectories (at least 1500) are run in order to obtain standard error bars that are smaller than 0.01 (one percentage point). The oxygen molecule is initially placed halfway between the two periodic images of the slab, with the azimuthal and polar angles sampled according to the rotational state[101] (see Section 2.4.2). Trajectories are considered to be reacted when the O_2 bond is extended beyond 1.59 Å for the HSE03-1/3X DF or 1.79 Å for the MS-RPBEl DF. Lowering the dissociation criterium for the MS-RPBEl DF from 1.79 Å to 1.59 Å does not affect S_0. When the distance between the molecule and the surface is larger than the initial value (7.5 Å for MS-RPBEl and 5 Å for HSE03-1/3X) and the velocity vector is pointing away from the surface, the trajectory is considered to be scattered. With the employed propagation time of 10 ps each trajectory ends with one of these two outcomes (i.e., trapping at the surface does not lead to ambiguous outcomes). Furthermore, the equations of motion are integrated with the Stoer and Bulirsch method, using a variable time step[102, 103] (see Section 2.2.1). In using the QCT method[74], the usual assumption is made that the dynamics calculations are not affected by problems related to zero-point energy conversion or the neglect of other quantum effects like tunneling. These assumptions have also been made in previous dynamics studies of the O_2 + Al(111) reaction[44, 64]. Quantum and quasi-classical studies of the CH_4 + Pt(111) system[104] suggest that these conditions should be met in QCT calculations of sticking probabilities exceeding 0.01, where sticking usually proceeds in a classical, over the barrier fashion.

5.4 Results

5.4.1 Potential Energy Surface

Table 5.2 compares several barrier heights and locations (i.e., the distance to the surface Z_{O_2}) obtained with ECW theory[64], the MS-RPBEl DF, and the HSE03-1/3X DF. Some of the trends in how the barrier height varies with the

TABLE 5.2: Barrier location (Z_{O_2}, Å) and height (E_b, kJ/mol) of O_2 on Al(111) obtained from raw ECW data[64], and the MS-RPBEl and HSE03-1/3X CRP PESs generated in this work. The nomenclature of the different orientations is taken from Ref. [64]. The zero-point energy corrected barriers are provided in the brackets.

		Z_{O_2} (Angstrom)			E_b (kJ/mol)		
site	orientation	ECW	MS-RPBEl	HSE03-1/3X	ECW	MS-RPBEl	HSE03-1/3X
fcc	//1	1.9	3.0	2.6	60	3.7 (3.7)	12.3 (12.9)
	//2	2.2	3.0	2.7	43	3.4 (2.0)	11.4 (10.7)
	//3	2.4	3.0	2.6	18	3.7 (1.0)	12.3 (10.0)
	$\perp$	1.9	3.0	2.8	41	8.8 (7.4)	26.9 (26.7)
top	//	2.6	2.8	2.6	64	9.3 (7.8)	22.2 (21.3)
	$\perp$	2.8	3.1	2.8	64	12.0 (10.6)	26.8 (26.8)
bridge	//	2.4	2.7	2.5	54	14.3 (12.9)	29.4 (28.8)
	$\perp$	2.7	3.2	2.9	43	7.3 (5.9)	19.4 (15.7)

impact site and orientation are rather different for ECW theory than for MS-RPBEl and HSE03-1/3X. Generally, both the barrier heights and the anisotropy are lower with the DFs than with ECW theory, and the discrepancies between MS-RPBEl and ECW theory are larger than between HSE03-1/3X and ECW theory. More specifically, among the barrier heights listed the minimum barriers are 3.4, 11.4, and 18 kJ/mol for the meta-GGA DF, the hybrid GGA DF, and ECW theory, respectively. Furthermore, the difference between the smallest and largest barrier heights listed, which measures how the barrier height varies with impact site (energetic corrugation) and molecular orientation (anisotropy) increases in the same order as 10.9, 17.1, and 46 kJ/mol, respectively. Qualitative predictions regarding the dependence of the sticking (or dissociative chemisorption) probability (S_0) on the incidence energy (E_i) can then be made with the hole model[105]. This model holds that $S_0(E_i)$ is proportional to the fraction of impact sites and orientations for which E_i exceeds the barrier height. The hole model then predicts that the meta-GGA DF yields the lowest energy threshold in the S_0 curve, while the highest threshold should be found for the ECW results, with the HSE03-1/3X threshold being intermediate. Additionally, based on the barrier height variation the model predicts the steepest S_0 curve for the meta-GGA DF and the slowest rising curve for the ECW method. Two-dimensional cuts through the computed PESs are shown for the minimum barrier geometry (i.e., the second parallel orientation at the fcc site) in Figures 5.3a (MS-RPBEl) and 5.3b (HSE03-1/3X).

5.4.2 Sticking Probability

The computed $S_0(E_i)$ curves shown in Figure 5.2a display the behavior predicted by the hole model on the basis of the barrier heights shown in Table 5.2. Here, the focus is on the overall sticking of O_2 on Al(111) even though this includes contributions from both dissociative chemisorption and abstraction[106]. The MS-RPBEl DF yields a qualitative improvement over the (R)PBE GGA DF by describing the reaction as activated, but with its low energy threshold and steep rise with E_i it still overestimates the reactivity considerably. The HSE03-1/3X DF yields considerably better agreement with experiment. The comparison suggests that the minimum barrier height is well-described with the HSE03-1/3X DF, although the slope of the sticking curve is still too steep. In line with the above the latter observation suggests that the anisotropy of the barrier height in θ and ϕ is underestimated and that the energetic corrugation of the barrier height may be too low. The too low anisotropy of the HSE03-1/3X PES also explains why the rotational alignment dependence of the sticking probability is underestimated, even though the calculations

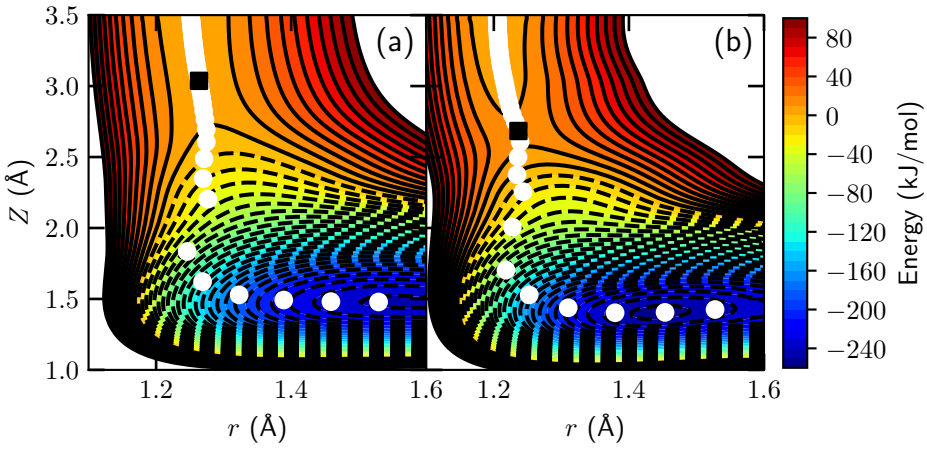

FIGURE 5.3: Elbow plot of the molecule-surface interaction energy of O_2 on Al(111) as a function of Z_{O_2} and r computed with the MS-RPBEl (a) and HSE03-1/3X (b) DFs for the second parallel configuration at the fcc site (see Ref. [64]). Black contour lines are drawn at an interval of 10 kJ/mol between -260 and 100 kJ/mol. The white circles indicate the MEP in reduced dimensionality and the black square indicates the highest point along the MEP. The zero of the energy corresponds to the gas phase equilibrium geometry of O_2.

qualitatively reproduce the dependence found experimentally (see Figure 5.2b, and Section 5.B.5 for further discussion). ECW theory yields the best overall agreement with experiment, especially regarding the slope. However, the reaction threshold appears to be better described with the tested hybrid functional, suggesting that the HSE03-1/3X minimum barrier height is more accurate than the ECW value. It is also noted that the ECW results are based on an approximately fitted FPLEPS PES whereas the dynamics results in this chapter are based on PESs accurately interpolating the DFT data with the CRP. Furthermore, the agreement of the ECW results with experiment at low incidence energies may have been improved artificially by simulating the reaction of non-rotating O_2 instead of using the appropriate rotational distribution[64] (see Figure 5.B.2 and Section 5.B.4).

The above conclusions are valid provided that the sticking is not much affected by electron-hole pair (ehp) excitation and surface atom motion, the effects of which could lower the energy threshold and the steepness of $S_0(E_i)$. These possible effects are believed to be unimportant for the following reasons. First, experimental results indicate that the surface temperature does not influence S_0[63]. Second, according to the local density friction approximation, the probability to excite ehps will only be high if the dynamics sample high electron densities. However, for O_2 + Al(111), the barrier is early (far away from the surface), so that the electron density sampled by O_2 before it encounters a barrier is low. Third, the location of the barrier far away from the surface also suggests small electronic and mechanical couplings[107, 108] with surface atom motion, i.e., the barrier height and location should not vary much with the motion of the nearest surface atom. According to the lattice relaxation sudden model[107, 108], surface atom motion should then not much affect S_0.

The reasonably good description of the minimum barrier obtained with the HSE03-1/3X DF is possibly due to the reduction of the delocalization error (or the SIE) as a fraction of exact exchange energy is included[39, 109–112]. Furthermore, the HSE03-1/3X DF also qualitatively reproduces experimental alignment and incidence angle dependent sticking probabilities (see Sections 5.B.5 and 5.B.6, respectively). It is concluded that the HSE03-1/3X DF already gives a reasonable description of the reaction of O_2 on Al(111), suggesting that an accurate SRP-DF for this system can be developed on the basis of screened hybrid DFs. As further discussed in Section 5.C.2, it is expected that a functional better describing the sticking in O_2 + Al(111) would contain a correlation function approximately describing the Van der Waals dispersion interaction[113–115], while α_X should then probably be increased in the hybrid functional.

5.4.3 Functional-Driven Error

We now come to a tentative explanation of why semi-local DFT may be quite accurate for barriers to dissociative chemisorption on metals if $(W - E_{ea}) > 7\,\text{eV}$. Some have recently suggested[8] a possible reason for this success in terms of the delocalization error of Yang and co-workers[38, 39, 41]. The explanation is necessarily of a hand waving nature, as delocalization errors, like self-interaction errors[111, 116], are usually hard to quantify for most systems of practical interest. The explanation takes its cue from the explanation of the GGA's tendency to underestimate gas phase barrier heights given in the introductory paragraphs of our letter. The explanation of the GGA's success in describing molecule-metal surface reactions that may be applied if $(W - E_{ea}) > 7\,\text{eV}$ runs as follows: The electrons coming from the molecule to form new bonds are too delocalized at the TS, and this leads to a delocalization error[41], but the electrons coming from the metal were already quite delocalized in the metal, and they become more localized at the TS, leading to a localization error. If electron transfer does not occur too easily (i.e., $(W - E_{ea}) > 7\,\text{eV}$), then apparently a cancellation of errors occurs, allowing one to tweak the barrier by mixing GGA-exchange-based DFs. Presumably, the cancellation effect disappears once $(W - E_{ea}) < 7\,\text{eV}$ and the electrons coming from the metal start to spill over to the molecule due to charge transfer. The diffuse charge distribution on the negatively charged molecule upsets the balance leading to too much electron delocalization and therefore an underestimation of the TS energy. The explanation finds quantitative support in the high Bader charges found on the molecules in the TSs of the difficult systems (see Table 5.B.6 and Section 5.B.3).

A remaining question concerns the origin of the delocalization error that plagues the accuracy of GGA barrier heights for systems with $(W - E_{ea}) < 7\,\text{eV}$, which is addressed here for O_2 + Al(111). There are two possibilities. First, it is possible that the change from reactants to the TS (at which the true electron density will usually be more delocalized) by itself drives the underestimation of the barrier height, i.e., that the error in the barrier height is functional driven[117, 118]. Second, the error may also come about, or be further increased, because semi-local functionals yield self-consistent electron densities at the TS that differ from the true densities to the extent that density driven errors, which may result from over-delocalization, result[117, 118]. The question is relevant: even for stretched H_2^+, which is a prototypical case for delocalization error[39], the error of GGAs is still predominantly functional-driven[119]. In other words, the self-consistent results are not much improved when GGAs are evaluated on the exact density of stretched H_2^+[119].

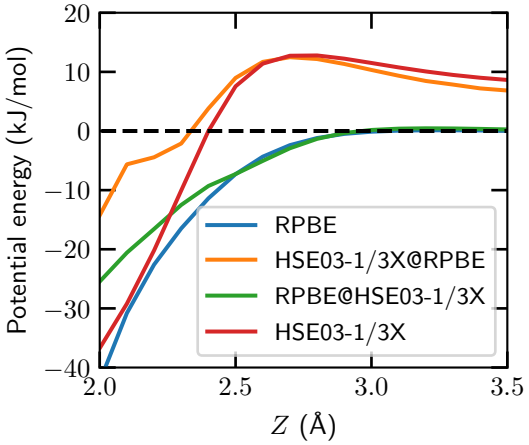

FIGURE 5.4: Potential energy of O_2 + Al(111) as a function of Z_{O_2} for $r = 1.25$ Å and the fcc //3 configuration computed self-consistently and non-self-consistently with the RPBE and HSE03-1/3X functionals applied to self-consistent RPBE and HSE03-1/3X electron densities.

To estimate the RPBE's density-driven error (DDE) for the barrier height of O_2 + Al(111), RPBE is evaluated on the presumably more accurate HSE03-1/3X DF electron density, i.e., RPBE@HSE03-1/3X. Interestingly, this yields almost the same barrier height as the self-consistent RPBE (see Figure 5.4). This shows, at least for the early barrier system investigated here, that the error of RPBE is functional-driven and not density-driven. At the same time, to a good approximation, the HSE03-1/3X@RPBE energy equals the HSE03-1/3X energy in the entrance and barrier region of the O_2 + Al(111) PES (see Figure 5.4 and Table 5.B.4). The results therefore show that the RPBE error in the barrier height is not due to "spuriously easy charge transfer" as suggested in Ref. [37] since this should be reflected in the RPBE density to which the HSE03-1/3X is applied in HSE03-1/3X@RPBE. The result that HSE03-1/3X@RPBE yields similar energies as HSE03-1/3X in the entrance and barrier regions of the O_2 + Al(111) PES suggests that the HSE03-1/3X@RPBE approach might accurately describe the sticking probability for this and other DC on metal systems. This is a potentially useful finding because, as discussed in Section 5.3, using the HSE03-1/3X@RPBE approach to compute energies is roughly an order of magnitude less expensive than using the HSE03-1/3X DF[120], with obvious implications for dynamics studies based on hybrid density functionals. While the DDE has a small contribution to the total RPBE error around the TS, its DDE becomes large when the molecule gets closer to the surface (see Figure 5.4 and Section 5.B.2). This finding is consistent with the results of Perdew and co-workers for molecular adsorption of CO on Pt(111), who also find that the DDE of semi-local DFT is large when the molecule is close to the surface[121].

5.5 Conclusion

In conclusion, comparison of experiment and DFT-based theory, and of DMC and RPBE DFT calculations for sticking of molecules on metal surfaces suggests that GGA-DFT starts to fail for molecule-metal surface reaction barriers when $(W - E_{ea}) < 7\,\text{eV}$. The results obtained for O_2 + Al(111) with the MS-RPBEl DF suggest that meta-GGA DFs of the "made simple (MS)" kind can slightly remedy the SIE problem, but not sufficiently for this system. Screened hybrid DFs like HSE03-1/3X, and its much cheaper HSE03-1/3X@RPBE alternative, offer a considerably improved description of O_2 + Al(111) in that they yield sticking probabilities in semi-quantitative agreement with experiment, thus offering more promise, as also implied by single point calculations performed at reaction barrier geometries of two other difficult systems (see Table 5.B.5 and Section 5.B.2). The HSE03-1/3X DF gives a good description of the reaction threshold but still overestimates the slope of the sticking probability curve for O_2 + Al(111). The results suggest that SRP-DFs can be built on the basis of screened hybrid exchange DFs for DC systems in which $(W - E_{ea}) < 7\,\text{eV}$, i.e., when electron transfer is facile. Such calculations have the potential to widen the scope of existing databases (now only SBH10[23]) of barriers for molecule-metal-surface systems. Indeed, it is likely that the choice of systems in this database (SBH10 contains only H_2-metal, CH_4-metal, and N_2-metal systems that are all in the green-blue part of the spectrum made up by Figure 5.1) has led to systematic bias: The inadvertent choice of systems for which GGA-based exchange works well may actually be responsible for the outcome[23] that the GGA-exchange-based DF performed better than the also tested meta-GGA and hybrid functionals. Even more importantly, the calculations referred to might also increase the range of heterogeneously catalyzed processes that may be simulated reliably based on accurate DFT calculations on the constituent elementary molecule-metal surface reactions.

Appendix

5.A Method

5.A.1 Density Functionals Used in This Chapter

The three DFs selected in this chapter are the RPBE DF (in the sense that its results serve as a yardstick to measure other results against), and the MS-RPBEl[75] and HSE03-1/3X[76, 77, 122] DFs used in the study of the dissociative chemisorption of O_2 on Al(111). Here, the choice of these functionals is briefly discussed.

The RPBE DF[16] may be viewed as a non-empirical GGA functional just like the PBE DF[14], as Hammer et al. made sure that the constraints imposed on the PBE DF are also imposed on the RPBE-DF[8, 14]. This includes the recovery of the uniform electron gas (UEG) limit, which ensures the functional's applicability to metals[123]. The RPBE DF, which was originally designed to improve the chemisorption energies of atoms and molecules on metals, which are severely overestimated with PBE, yields higher barriers for gas phase reaction barriers than PBE, thereby improving on their description (e.g., the mean unsigned error for the barrier heights in the HTBH38/08 and NHTBH38/08 databases is reduced from 8.9 to 6.6 kcal/mol going from PBE to RPBE[2]). The RPBE DF also yields consistently higher barriers for dissociative chemisorption reactions on metals[5, 7] than the PBE DF and, in fact, than any non-empirical GGA DF obeying the UEG limit that we know of. Hence, RPBE[16] (or RPBE-vdW-DF1[16, 124]) results are used as yardstick to measure other results for dissociative chemisorption systems against: if the RPBE (RPBE-vdW-DF1) DF yields a barrier that is too low, perhaps a meta-GGA but probably a hybrid DF will have to be used to obtain a higher barrier.

Some important advantages of the MS-RPBEl meta-GGA DF tested on O_2 + Al(111) have already been mentioned above. They include an approximate correction for one electron-self interaction, which is ensured by demanding that the functional reproduces the exact energy of the H-atom and the atomic/-molecular orbital limit. Based on this approximate correction one might expect

the functional to perform well on reaction barrier heights, the description of which may suffer from self-interaction errors[38, 39, 109]. The MS-RPBEl DF gives a chemically accurate description of the dissociative chemisorption of H_2 on Cu(111), and also a quite accurate description of that of H_2 on Ag(111)[75], which are additional reasons for including it here. The performance of this MS functional is in contrast to that of the meta-GGA MS2 DF[78], which, although based on similar design principles, with a mean signed error of −7.8 kcal/mol showed a rather poor performance on the dissociative chemisorption barriers in the SBH10 database[23].

The hybrid DF HSE03-1/3X that is applied to O_2 + Al(111) may be viewed as a re-parameterized version of HSE06[122]. HSE06 is a screened hybrid DF with an exact exchange ratio α_X equal to 0.25 as in the PBE0 DF[125, 126]; at very short range it equals PBE0 and at long range the PBE DF is obtained. As originally intended[76], the HSE03 DF (which at the start suffered from an implementation error[77]) is the HSE06 DF with a slightly different range parameter (0.15 bohr^{-1})[76] than used in HSE06 (0.11 bohr^{-1})[122]. However, the most important change made going from HSE06 to HSE03-1/3X is that a higher exact exchange ratio ($\alpha_X = 1/3$) is used than the value implemented originally in HSE06 and PBE0 (($\alpha_X = 1/4$)). Increasing the ratio of exact exchange in a hybrid DF is a longstanding[81–83] and accepted[3, 127] practice for improving its performance on gas phase reaction barrier heights. For example, the M08-SO and MO8-HX DFs[83] have $\alpha_X = 0.57$ and 0.52, respectively, and are among the best three performing functionals for the BH206 database[3]. An example that is pertinent to using HSE03-1/3X instead of HSE03, as done here, showed that changing α_X from 1/4 to 1/3 in PBE0 reduces the mean absolute error in the reaction barrier heights of the DBH24/08 database from 4.0 to 2.9 kcal/mol[80]. A more minor change made here to HSE06 mentioned already above is that a somewhat larger value is used for the screening parameter, i.e., the one corresponding to HSE03. Note that with the recommended VASP settings (screening parameters of 0.2 Å^{-1} ($\approx$ 0.106 bohr^{-1}) and 0.3 Å^{-1} ($\approx$ 0.159 bohr^{-1})) the settings used for HSE03 and HSE06 are actually a bit different than the ones in the original papers (0.11 and 0.15 bohr^{-1} for HSE06 and HSE03, respectively), but this slight difference should not affect the results much.

5.A.2 Work Function and Electron Affinity Values

The choice of how to compute the difference of the work function and the electron affinity ($W - E_{ea}$) has been a pragmatic one. The W-values in this chapter have been mostly taken from Ref. [128], which gives recommended

values for a number of metal surfaces based on an evaluation of experimental results, so here empirical values are used (see Table 5.A.1). The electron affinities have been mostly taken from a NIST database (Ref. [60]) using semi-empirical composite theory with the G4 basis set (see also Table 5.A.2). Note that the electron affinity of CH_4 is obtained by taking the difference between the exciplex state (−40.240 409 Hartree (−1094.9978 eV), see Table S3 of Ref. [129]) and the ground state (−40.451 691 Hartree (−1100.7471 eV), see Table S2 of Ref. [129]) energies obtained with CCSD(T)/aug-cc-pVQZ.

Of course, one might also want to use an all-DFT approach. Results of Perdew and co-workers[121] suggest that metal surface work functions can be computed with a mean absolute error of 0.16, 0.21, 0.11, 0.11, and 0.08 eV using the LDA[130, 131], PBE[14], PBEsol[132], SCAN[133], and SCAN+rVV10[134] DFs, respectively. Furthermore *W*-values computed for a large range of metal surfaces with DFT have been tabulated for the LDA, the PBE, and the RPBE[16] DFs in the supporting information of Ref. [135].

The calculation of electron affinities of small molecules is not so straightforward[129, 136, 137], and this is also true for DFT[137, 138]. This is especially true if the electron affinity is negative, which means that the anion is unstable with respect to the dissociation into the neutral molecule and a free electron, as the calculation of a metastable state state is then required (see, e.g., the calculation of the electron affinity of CH_4[129]). As can be seen from Table 5.A.2, this is true for all but one (O_2) of the molecules in the molecule-surface systems considered here. Studies that perform benchmarks on the thermochemistry of large numbers of DFs[2, 3] typically employ databases containing back corrected experimental electron affinities (G21EA)[137] or electron affinities computed with a high-level ab initio electronic structure method (EA13/03)[2], which exclusively or predominantly contain positive electron affinities of atoms and small molecules only. Given how complicated it is to compute negative electron affinities, it is recommended to simply use the results from Ref. [60] as obtained using semi-empirical composite theory with the G4 basis set (see Table 5.A.2), for reasons discussed in Ref. [129].

5.B Results

5.B.1 Self-Consistent DFT Results for O_2 + Al(111)

An one-dimensional cut through the HSE03-1/3X PES along the molecule-surface distance is shown in Figure 5.4 for the fcc //3 configuration and $r = 1.25$ Å, for which the barrier height is 12.3 kJ/mol (see Table 5.2). The barrier is found at $Z = 2.6$ Å. For this configuration and *r*-value, the total

TABLE 5.A.1: Work function values of several metal surfaces, which are taken from Ref. [128], except for the value for Pt(211), which is taken as the aforementioned value for Pt(111) plus the difference of calculated LDA values for Pt(211) and Pt(111) from Ref. [139].

Surface	Work function (eV)
Al(111)	4.32
Ni(111)	5.24
Au(111)	5.33
Ru(0001)	5.4
Cu(100)	4.73
Cu(111)	4.9
Pt(111)	5.91
Pt(211)	5.64

TABLE 5.A.2: Electron affinity values of several molecules, which are taken from Ref. [60] using semi-empirical composite theory with the G4 basis set, except for H_2O (CCSD(T) with a daug-cc-pVTZ basis set) and HCl (B97D3 DF with an aug-cc-pVTZ basis set), and except for CH_4, which is taken from Ref. [129].

Surface	Electron affinity (eV)
CH_4	-5.75
H_2	-3.155
O_2	0.463
HCl	-0.514
N_2	-1.982
NH_3	-0.897
H_2O	-0.181

TABLE 5.B.1: Minimum barrier heights and bulk lattice constants computed with different variations of the screened hybrid PBE DF, i.e., different exact exchange ratios and screening length parameters are employed. The barrier is taken to be at $Z = 2.8$ Å, $r = 1.25$ Å, and in the fcc //3 configuration. The row shown in bold face lists the functional used in the dynamics calculations, and presents the results obtained with it. The experimental value of the lattice constant is 4.032 Å[97].

DF	Exact exchange ratio	Screening length parameter ($Å^{-1}$)	Bulk lattice constant (Å)	E_b (kJ/mol)
HSE06[122]	1/4	0.2	4.023	7.9
HSE06-1/3X	1/3	0.2	4.018	13.2
HSE06-1/2X	1/2	0.2	4.009	25.0
HSE03-1/3X	**1/3**	**0.3**	**4.022**	**12.8**
RSX-PBE0[140]	1/4	0.39	4.029	3.6
RSX-PBE0-1/3[140]	1/3	0.37	4.025	11.4

magnetic moment (i.e., the number of unpaired electrons) of the O_2 + Al(111) system as a function of Z for $r = 1.25$ Å and the fcc //3 orientation is shown in Figure 5.B.1. The magnetic moment is an indicator of charge transfer in the sense that a spin-flip and concomitant change in magnetic moment can only take place after charge transfer from the surface to the molecule has occurred[37]. Here, it can be seen that when a DF is employed that (roughly) corrects for the SIE (i.e., HSE03-1/3X), the magnetic moment drops more gradually when approaching the surface than with the standard RPBE DF. Previously, this effect has also been shown for the charge of O_2 approaching an Al_5 cluster using (screened) hybrid DFs[68]. Furthermore, from visual inspection it is observed that the charge density is more localized on the O_2 molecule when employing SIE-correcting DFs than when using the RPBE DF (results not shown here).

How the barrier height for O_2 + Al(111) depends on the parameters of the HSE functional used here is investigated as well. As Table 5.B.1 shows, the barrier height is rather insensitive to changing the screening parameter (i.e., using HSE03-1/3X rather than HSE06-1/3X changes the barrier height by just 0.4 kJ/mol), while increasing α_X from 1/4 to 1/3 to 1/2 leads to clear increases in the barrier height, as one would expect from the discussion in Section 5.A.1. Increasing the exact exchange ratio also decreases the lattice constant of Al somewhat, while the lattice constant is not much affected by changing the screening length parameter (Table 5.B.1).

TABLE 5.B.2: Vibrational frequencies of the molecule at the reaction barrier geometries (see Table 5.2). Total zero point vibrational energies (ZPE) are also listed. Results are obtained from the HSE03-1/3X PES. The nomenclature of the different configurations is taken from Ref. [64].

site	orientation	Vibrational mode (meV) 1	2	3	4	5	6	ZPE (meV)
fcc	//1	138.4	18.5	8.2	5.9i	17.4i	87.2i	82.6
	//2	121.0	12.8	8.8	4.4i	15.7i	121.0i	71.3
	//3	89.5	14.9	4.1i	14.1i	18.8i	138.4i	52.2
	⊥	106.5	20.7	1.0	2.9i	20.6i	106.4i	64.1
top	//	115.6	14.9	5.9	5.9i	14.7i	115.6i	68.2
	⊥	131.2	21.8	1.1	0.9i	21.8i	131.2i	77.1
bridge	//	107.6	17.1	7.0	7.9i	15.6i	107.6i	65.9
	⊥	113.8	15.3	2.6	1.6i	15.9i	113.7i	65.9
gas phase		153.0	-	-	-	-	-	76.5

TABLE 5.B.3: Same as Table 5.B.2 but results are obtained from the MS-RPBEl PES.

site	orientation	Vibrational mode (meV) 1	2	3	4	5	6	ZPE (meV)
fcc	//1	142.2	4.7	3.3	3.8i	5.8i	89.6i	75.1
	//2	118.9	3.9	2.6	3.9i	4.6i	118.9i	62.7
	//3	89.4	6.5	5.9	3.6i	5.6i	142.5i	50.9
	⊥	111.4	9.3	2.8	5.5i	9.1i	111.7i	61.8
top	//	113.3	8.3	0.9	4.3i	7.0i	113.3i	61.3
	⊥	115.9	8.1	0.1	2.0i	7.9i	115.9i	62.1
bridge	//	102.7	9.6	5.5	6.0i	8.6i	102.7i	58.9
	⊥	115.6	6.4	0.6	1.4i	6.9i	115.5i	61.3
gas phase		146.6	-	-	-	-	-	73.3

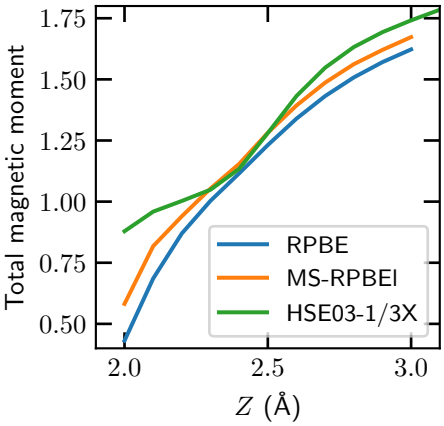

FIGURE 5.B.1: Total magnetic moment of the O_2 + Al(111) system as a function of Z_{O_2} for $r = 1.25$ Å and the fcc //3 configuration using several DFs.

5.B.2 Non-Self-Consistent DFT Results for O_2 + Al(111), HCl + Au(111), and NH_3 + Ru(0001)

The barrier heights resulting from non-self-consistent calculations employing a self-consistent density from a different DF, as described in Ref. [117, 118], are shown in Table 5.B.4 for O_2 + Al(111). Interestingly, the non-self-consistent calculations yield similar barrier energies as the self-consistent calculations (see also Figure 5.4). As discussed above, this implies that even when a different electron density is employed, the relative energy does not change considerably; i.e., the failure of RPBE in yielding an accurate adiabatic barrier for O_2 + Al(111) is not caused by a density-driven error but by a functional-driven error. Only when the molecule is closer to the surface (i.e., the value of Z is lower) does the density driven error play a considerable role. Interestingly, the appearance of the density driven error (see Figure 5.4) coincides with an increasing difference of the magnetic moment between HSE03-1/3X and RPBE (see Figure 5.B.1).

Non-self-consistent calculations of the same kind have also been performed for HCl + Au(111) and NH_3 + Ru(0001) (see Table 5.B.5). In general, increasing the fraction of exact exchange, and therefore diminishing the amount of semi-local PBE exchange, leads to barrier heights higher than those found with PBE. These results suggest that employing screened hybrid DFs to systems where $(W - E_{ea}) < 7\,\text{eV}$ may improve the comparison between theory and experiment compared to that obtained with GGA DFs. The barrier for NH_3 + Ru(0001) obtained with non-self-consistent HSE calculations is not yet higher than the previous RPBE-vdW-DF1 result (Table 5.B.5), but this will

TABLE 5.B.4: Barrier height (in kJ/mol) of O_2 on Al(111) obtained from the HSE03-1/3X CRP PES and HSE03-1/3X@RPBE calculations. The nomenclature of the different configurations is taken from Ref. [64].

site	orientation	$E_{b,\text{HSE03-1/3X}}$	$E_{b,\text{HSE03-1/3X@RPBE}}$
fcc	//1	12.3	11.5
	//2	11.4	10.3
	//3	12.3	11.4
	$\perp$	26.9	30.1
top	//	22.2	21.5
	$\perp$	26.8	29.0
bridge	//	29.4	31.1
	$\perp$	19.4	22.7

probably change if a screened hybrid function is used that employs semi-local RPBE exchange instead of PBE exchange. The barrier obtained with the HSE03@RPBE-vdW-DF1 approach for HCl + Au(111) is higher than those obtained with any semi-local exchange functional tested thus far (see Table 3.4, the highest barrier (101.3 kJ/mol) thus far was obtained with RPBE), which should help to get better agreement between theory and experiment for this system.

5.B.3 Correlation Between $(W - E_{ea})$ and Charge Transfer at the TS

The excess charge at the molecule for the TS of several molecule-metal surface systems (i.e., the charge transferred from the metal surface to the molecule) is shown in Table 5.B.6. The results show a clear correlation between the amount of charge transferred to the molecule and the difference between the work function and the electron affinity; i.e., when $(W - E_{ea})$ decreases, the amount of excess negative charge on the molecule increases. One might then also argue that the barriers of the difficult systems should be too low because the difficult systems are affected by charge transfer at the barrier, as semi-local functionals may severely overestimate the interaction of charge transfer complexes[38].

5.B.4 Dynamics: Dependence of S_0 on Molecular Beam Conditions

The sticking probability in Figure 5.1 is obtained for a simulated mono-energetic molecular beam. Simulation of only a single energy instead of a velocity distribution does not affect results considerably for weakly activated

TABLE 5.B.5: Barrier heights (in kJ/mol) obtained self-consistently and non-self-consistently for three of the five difficult systems discussed in this chapter (see Figure 5.1). All calculations are performed for a 2×2 supercell, $8 \times 8 \times 1$ k-point grid and a kinetic energy cut-off of 400 eV.

System	DF	$E_{b,DF}$	$E_{b,HSE03\text{-}1/3X@DF}$	$E_{b,HSE03\text{-}1/2X@DF}$	$E_{b,PBE}$	$W - E_{ea}$ (eV)	Excess charge (e^-)
Al(111) + O_2	RPBE	0.1	12.5	29.9	-	3.857	0.332
Au(111) + HCl[29]	RPBE-vdW-DF1	85.1	106.2	122.9	72.9	5.844	0.318
Ru(0001) + NH_3[30]	RPBE-vdW-DF1	68.6	53.8	60.6	38.7	6.297	0.348

TABLE 5.B.6: Excess charge at the molecule for the TS compared to a neutral molecule for several systems obtained with the Bader charge decomposition scheme.

System	DF	$W - E_{ea}$ (eV)	Excess charge (e^-)
Al(111) + O_2	HSE03-1/3X	3.857	0.332
Ni(111) + H_2O[141]	SRP32-vdW-DF1	5.421	0.472
Au(111) + HCl[26]	RPBE	5.844	0.348
Ru(0001) + NH_3[30]	SRP32-vdW-DF1	6.297	0.348
Cu(111) + H_2[142]	SRP48	8.055	0.229
Pt(111) + H_2[10]	PBEa57-vdW-DF2	9.065	-0.047
Ni(111) + CH_4[8]	SRP32-vdW-DF1	10.99	0.241

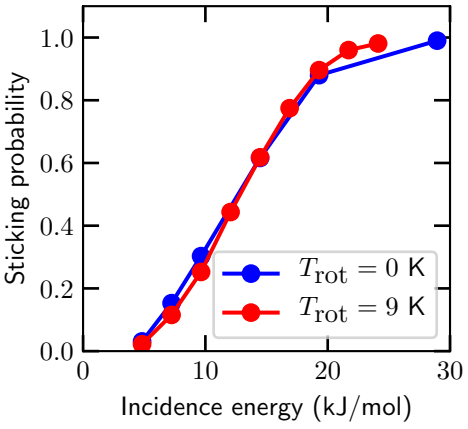

FIGURE 5.B.2: Sticking probability of O_2 on Al(111) as a function of translational energy for normal incidence. The blue circles indicate results for O_2 in the rovibrational ground state, whereas the red circles indicate results for a rovibrational state population according to $T_{vib} = 300\,K$ and $T_{rot} = 9\,K$.

systems[143]. The rovibrational state population is sampled according to a Boltzmann-like distribution (see for example Ref. [144]), where it is assumed that the vibrational temperature (T_{vib}) = 300 K and the rotational temperature (T_{rot}) = 9 K, as should be appropriate[145] for supersonic molecular beams containing O_2 and using a room temperature nozzle[63]. Simulating only the rotational ground state of O_2 instead of the distribution according to T_{rot} should lead to a too high sticking probability at low incidence energies (this is true even for a rotationally cold beam, see Figure 5.B.2), as is also confirmed by experiment[106]. Moreover, even though T_{vib} = 300 K is simulated, the population of the vibrational excited states is negligible (0.1%), and therefore the results for the simulated molecular beam can be considered to be for O_2 in the vibrational ground state. Since the previous results obtained with the FPLEPS PES based on ECW data are for O_2 in the rotational ground state[64], the agreement between the reactivity obtained with the ECW method and the experiments may well have been artificially improved somewhat for low E_i in this way (see Figure 5.B.2).

5.B.5 Dynamics: Dependence of S_0 on the Alignment of O_2

Figure 5.2b shows the sticking probabilities of O_2 in the helicopter, random, and perpendicular orientations relative to the surface (see Ref. [64] for explanations of the orientation distributions), as obtained experimentally and with the HSE03-1/3X DF. Note that different incident energy distributions (and, indeed, incidence energies) have been simulated than employed in the experiment as Kurahashi et al. did not publish experimentally determined beam parameters[65], and that the HSE03-1/3X DF yields a sticking probability of unity for $E_i > 25$ kJ/mol. Qualitatively, the simulations reproduce the experimental alignment trends[65]: The helicopter orientation is the most reactive one, whereas the perpendicular orientation is least reactive. Quantitatively, the differences between the sticking probabilities obtained for different alignments appear smaller in the theory than in the experiment. This observation gives support to the argument that the slope of the sticking probability curve computed with the HSE03-1/3X DF may be too high because the computed anisotropy of the barrier height at the minimum barrier impact site and at other impact sites is too low.

5.B.6 Dynamics: Dependence of S_0 on Incidence Angle

Figure 5.B.3 shows the sticking probability of off-normal incident O_2 on Al(111), where the normal incidence energy is computed as

$$E_{\text{normal}} = \cos^2(\theta) E_{\text{i}}. \tag{5.1}$$

Experimental trends in the sticking probability as a function of incidence angle of O_2 in its helicopter and cartwheel orientations are reproduced (see Figure 5.B.3a). Furthermore, normal energy scaling (NES)[146] is observed both experimentally and in this work (Figure 5.B.3a), while ECW theory slightly deviates from NES (Figure 5.B.3b).

5.C Discussion

5.C.1 O_2 + Metal Systems That Are Useful Benchmark Systems for Dissociative Chemisorption

Systems that are useful as benchmarks for dissociative chemisorption exhibit activated dissociation, so that sticking probabilities measured in molecular beam experiments increase with incidence energy[43]. Ideally, the dissociation is not affected by precursor dynamics, and the dissociative chemisorption probability rises to several tens of percent. Unfortunately, there are few O_2-metal systems exhibiting this simple behavior that we know of. As discussed in a recent review paper[147], many O_2-metal surface systems exhibit precursor dynamics, where O_2 first adsorbs molecularly as a superoxo- and/or peroxo-state, and only then dissociates. This complicates the analysis of the dissociation of O_2 on all group 10 metals (Ni, Pd, and Pt)[147]. While it has been known for some time that DFT with GGA functionals can be used to compute properties of these precursor states in reasonable agreement with experiments and that barriers to dissociation can be computed[148, 149], comparison of the latter to experimental values is very difficult, and it is hard to establish the reliability of experimental values of barrier heights, which may differ depending on the technique used and the analysis of the experiments[147]. Studies of the O_2 + Pt(111) system[150, 151] show how difficult it is to extract information on the dissociative chemisorption in this system, which is activated through thermal fluctuations at low surface temperature[151]."

Extracting accurate information on dissociative chemisorption of O_2 on the group 11 metals Ag and Au likewise is extremely difficult. Au surfaces show very high barriers to O_2 dissociation[147]. As discussed by Juaristi and co-workers, the major disagreement now seen in dynamics calculations on the

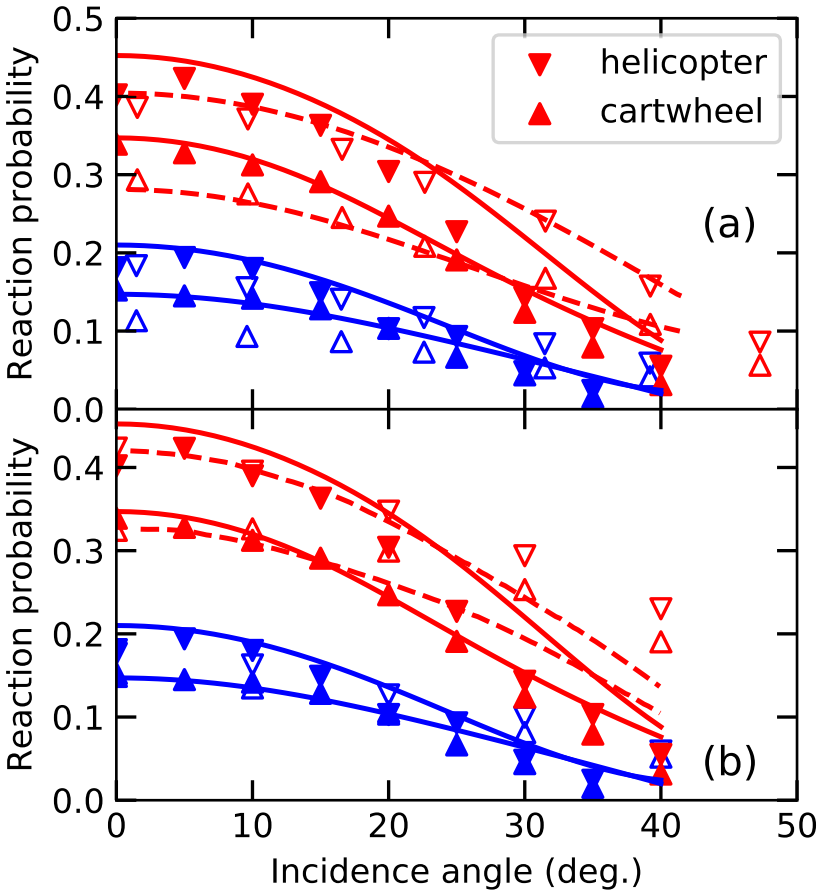

FIGURE 5.B.3: Sticking probability of O_2 ($v = 0, J = 2, K = 1$) on Al(111) as a function of incidence angle (degrees). (a) The solid symbols and lines indicate results obtained with the HSE03-1/3X DF for $E_i = 8.2\,kJ/mol$ (blue) and $E_i = 11.1\,kJ/mol$ (red). The open symbols and dashed lines indicate results from experiment[65] for $E_i = 9.6\,kJ/mol$ (blue) and $E_i = 17.4\,kJ/mol$ (red). The downward and upward pointing triangles correspond to the helicopter and cartwheel orientations, respectively. The lines correspond to results obtained with the assumption of normal energy scaling. (b) Same as panel a, but instead of experimental results, the results from a FPLEPS PES based on ECW data[64] for $E_i = 14.5\,kJ/mol$ (blue) and $E_i = 22.2\,kJ/mol$ (red) are shown. In both cases, the incidence energies in the calculations have been chosen such that similar reaction probabilities are obtained in the calculations as in the experiments.

dissociative chemisorption of O_2 on Ag(110), Ag(100), and Ag(111) is due to the difficulty on unraveling the contributions of molecular and dissociative chemisorption to sticking (see Figure 11 of their work)[152].

The only O_2-metal systems we are aware of that obey the following two conditions that (i) the sticking is activated, not precursor-mediated in a major way, and results in dissociative chemisorption with sticking probabilities equal to a few tens of percent, and that (ii) dynamics calculations using the RPBE density functional have been performed are the O_2 + Al(111)[44] example discussed extensively in this chapter, O_2 + Cu(111)[27], and O_2 + CuML/Ru(0001)[27]. In all cases, the dynamics calculations using a RPBE PES substantially overestimated the sticking probability. In the calculations on Cu and Cu/Ru surfaces, the effect of surface atom motion and surface temperature was modeled in an approximate manner, using the GLO model[27].

5.C.2 Towards an SRP Density Functional for O_2 + Al(111)

The HSE03-1/3X DF clearly is not yet an SRP DF for O_2 + Al(111). The suggestions below are based on how a SRP-DF may be developed in view of the following observations: (i) Compared to the ECW barrier geometries, the HSE03-1/3X geometries are too early, i.e., the barriers occur too far from the surface, and (ii) the too steep slope in the $S_0(E_i)$ curves obtained with standard GGA exchange-correlation DFs for H_2 + Ru(0001), which is also an early barrier system, could be remedied[7] by using correlation functionals approximately describing the attractive van der Waals dispersion interaction[124, 153].

We therefore suggest to proceed with the development of an SRP DF for O_2 + Al(111) as follows. First, the correlation DF in HSE03 (or alternatively HSE06), i.e., the PBE correlation DF, can be replaced with a Van der Waals correlation functional, obvious candidates being the vdW DFs developed for hybrids by Hyldgaard and co-workers[113, 114]. Alternatively, one could add the TS-vdW correction as used by Tkatchenko and co-workers to the HSE03 functional[115]. This would probably move the barrier geometries closer to the surface when compared to the HSE03-1/3X geometries. In turn, this would also increase the energetic corrugation and the anisotropy of the barrier heights, and lower the barrier heights. While the former change would probably result in better agreement with experiment for the steepness and the alignment dependence of $S_0(E_i)$ (Figures 5.2a and 5.2b, respectively), the energetic threshold of $S_0(E_i)$ would probably also be decreased, possibly resulting in worse agreement with experiment. However, this can probably be offset by increasing the fraction of exact exchange in HSE03 (see Section

5.B.1). Alternatively, one might think of replacing (a fraction of) the local PBE exchange[14] in HSE03 with RPBE exchange[16]. Finally, a screened meta-GGA hybrid DF might perform better[154] than a screened GGA hybrid DF. Especially a meta-GGA DF of the MS kind could perform well, as the MS-RPBEl DF already has shown to improve results for O_2 + Al(111) compared to the RPBE DF. Furthermore, using screened hybrid DFs where the range-separation parameter is either optimally pre-tuned (or self-consistently during calculations) or constrained to reproduce the energy of a free hydrogen atom could also improve results[85, 140, 155–158]. It is expected that the approaches sketched can go a long way towards improving the results for O_2 + Al(111), and developing an SRP DF for this system.

References

(1) Pribram-Jones, A.; Gross, D. A.; Burke, K. DFT: A Theory Full of Holes? *Annu. Rev. Phys. Chem.* **2015**, *66*, 283–304, DOI: 10.1146/annurev-physchem-040214-121420.

(2) Peverati, R.; Truhlar, D. G. Quest for a Universal Density Functional: The Accuracy of Density Functionals across a Broad Spectrum of Databases in Chemistry and Physics. *Philos. Trans. R. Soc. A* **2014**, *372*, 20120476, DOI: 10.1098/rsta.2012.0476.

(3) Mardirossian, N.; Head-Gordon, M. Thirty Years of Density Functional Theory in Computational Chemistry: An Overview and Extensive Assessment of 200 Density Functionals. *Mol. Phys.* **2017**, *115*, 2315–2372, DOI: 10.1080/00268976.2017.1333644.

(4) Janesko, B. G. In *Density Functionals: Thermochemistry*, Johnson, E. R., Ed.; Topics in Current Chemistry, Vol. 365; Springer International Publishing: Cham, 2015, pp 25–51, DOI: 10.1007/128_2014_555.

(5) Díaz, C.; Pijper, E.; Olsen, R. A.; Busnengo, H. F.; Auerbach, D. J.; Kroes, G. J. Chemically Accurate Simulation of a Prototypical Surface Reaction: H_2 Dissociation on Cu(111). *Science* **2009**, *326*, 832–834, DOI: 10.1126/science.1178722.

(6) Sementa, L.; Wijzenbroek, M.; van Kolck, B. J.; Somers, M. F.; Al-Halabi, A.; Busnengo, H. F.; Olsen, R. A.; Kroes, G. J.; Rutkowski, M.; Thewes, C.; Kleimeier, N. F.; Zacharias, H. Reactive Scattering of H_2 from Cu(100): Comparison of Dynamics Calculations Based on the Specific Reaction Parameter Approach to Density Functional Theory with Experiment. *J. Chem. Phys.* **2013**, *138*, 044708, DOI: 10.1063/1.4776224.

(7) Wijzenbroek, M.; Kroes, G. J. The Effect of the Exchange-Correlation Functional on H_2 Dissociation on Ru(0001). *J. Chem. Phys.* **2014**, *140*, 084702, DOI: 10.1063/1.4865946.

(8) Nattino, F.; Migliorini, D.; Kroes, G.-J.; Dombrowski, E.; High, E. A.; Killelea, D. R.; Utz, A. L. Chemically Accurate Simulation of a Polyatomic Molecule-Metal Surface Reaction. *J. Phys. Chem. Lett.* **2016**, *7*, 2402–2406, DOI: 10.1021/acs.jpclett.6b01022.

(9) Migliorini, D.; Chadwick, H.; Nattino, F.; Gutiérrez-González, A.; Dombrowski, E.; High, E. A.; Guo, H.; Utz, A. L.; Jackson, B.; Beck, R. D.; Kroes, G.-J. Surface Reaction Barriometry: Methane Dissociation on Flat and Stepped Transition-Metal Surfaces. *J. Phys. Chem. Lett.* **2017**, *8*, 4177–4182, DOI: 10.1021/acs.jpclett.7b01905.

(10) Ghassemi, E. N.; Wijzenbroek, M.; Somers, M. F.; Kroes, G.-J. Chemically Accurate Simulation of Dissociative Chemisorption of D_2 on Pt(111). *Chem. Phys. Lett.* **2017**, *683*, 329–335, DOI: 10.1016/j.cplett.2016.12.059.

(11) Spiering, P.; Shakouri, K.; Behler, J.; Kroes, G.-J.; Meyer, J. Orbital-Dependent Electronic Friction Significantly Affects the Description of Reactive Scattering of N_2 from Ru(0001). *J. Phys. Chem. Lett.* **2019**, *10*, 2957–2962, DOI: 10.1021/acs.jpclett.9b00523.

(12) Ghassemi, E. N.; Smeets, E. W. F.; Somers, M. F.; Kroes, G.-J.; Groot, I. M. N.; Juurlink, L. B. F.; Füchsel, G. Transferability of the Specific Reaction Parameter Density Functional for H_2 + Pt(111) to H_2 + Pt(211). *J. Phys. Chem. C* **2019**, *123*, 2973–2986, DOI: 10.1021/acs.jpcc.8b11018.

(13) Tchakoua, T.; Smeets, E. W. F.; Somers, M.; Kroes, G.-J. Toward a Specific Reaction Parameter Density Functional for H_2 + Ni(111): Comparison of Theory with Molecular Beam Sticking Experiments. *J. Phys. Chem. C* **2019**, *123*, 20420–20433, DOI: 10.1021/acs.jpcc.9b05928.

(14) Perdew, J. P.; Burke, K.; Ernzerhof, M. Generalized Gradient Approximation Made Simple. *Phys. Rev. Lett.* **1996**, *77*, 3865–3868, DOI: 10.1103/PhysRevLett.77.3865.

(15) Perdew, J. P.; Chevary, J. A.; Vosko, S. H.; Jackson, K. A.; Pederson, M. R.; Singh, D. J.; Fiolhais, C. Atoms, Molecules, Solids, and Surfaces: Applications of the Generalized Gradient Approximation for Exchange and Correlation. *Phys. Rev. B* **1992**, *46*, 6671–6687, DOI: 10.1103/PhysRevB.46.6671.

(16) Hammer, B.; Hansen, L. B.; Nørskov, J. K. Improved Adsorption Energetics within Density-Functional Theory Using Revised Perdew-Burke-Ernzerhof Functionals. *Phys. Rev. B* **1999**, *59*, 7413–7421, DOI: 10.1103/PhysRevB.59.7413.

(17) Jackson, B.; Nave, S. The Dissociative Chemisorption of Methane on Ni(100): Reaction Path Description of Mode-Selective Chemistry. *J. Chem. Phys.* **2011**, *135*, 114701, DOI: 10.1063/1.3634073.

(18) Jiang, B.; Liu, R.; Li, J.; Xie, D.; Yang, M.; Guo, H. Mode Selectivity in Methane Dissociative Chemisorption on Ni(111). *Chem. Sci.* **2013**, *4*, 3249–3254, DOI: 10.1039/C3SC51040A.

(19) Shen, X.; Zhang, Z.; Zhang, D. H. Communication: Methane Dissociation on Ni(111) Surface: Importance of Azimuth and Surface Impact Site. *J. Chem. Phys.* **2016**, *144*, 101101, DOI: 10.1063/1.4943128.

(20) Guo, H.; Jackson, B. Mode-Selective Chemistry on Metal Surfaces: The Dissociative Chemisorption of CH_4 on Pt(111). *J. Chem. Phys.* **2016**, *144*, 184709, DOI: 10.1063/1.4948941.

(21) Moiraghi, R.; Lozano, A.; Peterson, E.; Utz, A.; Dong, W.; Busnengo, H. F. Nonthermalized Precursor-Mediated Dissociative Chemisorption at High Catalysis Temperatures. *J. Phys. Chem. Lett.* **2020**, *11*, 2211–2218, DOI: 10.1021/acs.jpclett.0c00260.

(22) Wellendorff, J.; Lundgaard, K. T.; Møgelhøj, A.; Petzold, V.; Landis, D. D.; Nørskov, J. K.; Bligaard, T.; Jacobsen, K. W. Density Functionals for Surface Science: Exchange-Correlation Model Development with Bayesian Error Estimation. *Phys. Rev. B* **2012**, *85*, 235149, DOI: 10.1103/PhysRevB.85.235149.

(23) Mallikarjun Sharada, S.; Bligaard, T.; Luntz, A. C.; Kroes, G.-J.; Nørskov, J. K. SBH10: A Benchmark Database of Barrier Heights on Transition Metal Surfaces. *J. Phys. Chem. C* **2017**, *121*, 19807–19815, DOI: 10.1021/acs.jpcc.7b05677.

(24) Schimka, L.; Harl, J.; Stroppa, A.; Grüneis, A.; Marsman, M.; Mittendorfer, F.; Kresse, G. Accurate Surface and Adsorption Energies from Many-Body Perturbation Theory. *Nat. Mater.* **2010**, *9*, 741–744, DOI: 10.1038/nmat2806.

(25) Behler, J.; Delley, B.; Lorenz, S.; Reuter, K.; Scheffler, M. Dissociation of O_2 at Al(111): The Role of Spin Selection Rules. *Phys. Rev. Lett.* **2005**, *94*, 036104, DOI: 10.1103/PhysRevLett.94.036104.

(26) Füchsel, G.; del Cueto, M.; Díaz, C.; Kroes, G.-J. Enigmatic HCl + Au(111) Reaction: A Puzzle for Theory and Experiment. *J. Phys. Chem. C* **2016**, *120*, 25760–25779, DOI: 10.1021/acs.jpcc.6b07453.

(27) Ramos, M.; Díaz, C.; Martínez, A. E.; Busnengo, H. F.; Martín, F. Dissociative and Non-Dissociative Adsorption of O_2 on Cu(111) and Cu_{ML}/Ru(0001) Surfaces: Adiabaticity Takes Over. *Phys. Chem. Chem. Phys.* **2017**, *19*, 10217–10221, DOI: 10.1039/C7CP00753A.

(28) Hu, X.; Yang, M.; Xie, D.; Guo, H. Vibrational Enhancement in the Dynamics of Ammonia Dissociative Chemisorption on Ru(0001). *J. Chem. Phys.* **2018**, *149*, 044703, DOI: 10.1063/1.5043517.

(29) Füchsel, G.; Zhou, X.; Jiang, B.; Juaristi, J. I.; Alducin, M.; Guo, H.; Kroes, G.-J. Reactive and Nonreactive Scattering of HCl from Au(111): An Ab Initio Molecular Dynamics Study. *J. Phys. Chem. C* **2019**, *123*, 2287–2299, DOI: 10.1021/acs.jpcc.8b10686.

(30) Gerrits, N.; Kroes, G.-J. Curious Mechanism of the Dissociative Chemisorption of Ammonia on Ru(0001). *J. Phys. Chem. C* **2019**, *123*, 28291–28300, DOI: 10.1021/acs.jpcc.9b09121.

(31) Ertl, G. Elementary Steps in Heterogeneous Catalysis. *Angew. Chem. Int. Ed.* **1990**, *29*, 1219–1227, DOI: 10.1002/anie.199012191.

(32) Sabbe, M. K.; Reyniers, M.-F.; Reuter, K. First-Principles Kinetic Modeling in Heterogeneous Catalysis: An Industrial Perspective on Best-Practice, Gaps and Needs. *Catal. Sci. Technol.* **2012**, *2*, 2010–2024, DOI: 10.1039/C2CY20261A.

(33) Wolcott, C. A.; Medford, A. J.; Studt, F.; Campbell, C. T. Degree of Rate Control Approach to Computational Catalyst Screening. *J. Catal.* **2015**, *330*, 197–207, DOI: 10.1016/j.jcat.2015.07.015.

(34) Ertl, G. Primary Steps in Catalytic Synthesis of Ammonia. *J. Vac. Sci. Technol. A* **1983**, *1*, 1247–1253, DOI: 10.1116/1.572299.

(35) Rostrup-Nielsen, J. R.; Sehested, J.; Nørskov, J. K. In *Advances in Catalysis*; Academic Press: 2002; Vol. 47, pp 65–139, DOI: 10.1016/S0360-0564(02)47006-X.

(36) Perdew, J. P.; Ruzsinszky, A.; Constantin, L. A.; Sun, J.; Csonka, G. I. Some Fundamental Issues in Ground-State Density Functional Theory: A Guide for the Perplexed. *J. Chem. Theory Comput.* **2009**, *5*, 902–908, DOI: 10.1021/ct800531s.

(37) Libisch, F.; Huang, C.; Liao, P.; Pavone, M.; Carter, E. A. Origin of the Energy Barrier to Chemical Reactions of O_2 on Al(111): Evidence for Charge Transfer, Not Spin Selection. *Phys. Rev. Lett.* **2012**, *109*, 198303, DOI: 10.1103/PhysRevLett.109.198303.

(38) Zhang, Y.; Yang, W. A Challenge for Density Functionals: Self-Interaction Error Increases for Systems with a Noninteger Number of Electrons. *J. Chem. Phys.* **1998**, *109*, 2604–2608, DOI: 10.1063/1.476859.

(39) Cohen, A. J.; Mori-Sánchez, P.; Yang, W. Insights into Current Limitations of Density Functional Theory. *Science* **2008**, *321*, 792–794, DOI: 10.1126/science.1158722.

(40) Perdew, J. P.; Parr, R. G.; Levy, M.; Balduz, J. L. Density-Functional Theory for Fractional Particle Number: Derivative Discontinuities of the Energy. *Phys. Rev. Lett.* **1982**, *49*, 1691–1694, DOI: 10.1103/PhysRevLett.49.1691.

(41) Li, C.; Zheng, X.; Su, N. Q.; Yang, W. Localized Orbital Scaling Correction for Systematic Elimination of Delocalization Error in Density Functional Approximations. *Natl. Sci. Rev.* **2018**, *5*, 203–215, DOI: 10.1093/nsr/nwx111.

(42) Perdew, J. P.; Zunger, A. Self-Interaction Correction to Density-Functional Approximations for Many-Electron Systems. *Phys. Rev. B* **1981**, *23*, 5048–5079, DOI: 10.1103/PhysRevB.23.5048.

(43) Kroes, G.-J. Toward a Database of Chemically Accurate Barrier Heights for Reactions of Molecules with Metal Surfaces. *J. Phys. Chem. Lett.* **2015**, *6*, 4106–4114, DOI: 10.1021/acs.jpclett.5b01344.

(44) Behler, J.; Reuter, K.; Scheffler, M. Nonadiabatic Effects in the Dissociation of Oxygen Molecules at the Al(111) Surface. *Phys. Rev. B* **2008**, *77*, 115421, DOI: 10.1103/PhysRevB.77.115421.

(45) Liu, T.; Fu, B.; Zhang, D. H. HCl Dissociating on a Rigid Au(111) Surface: A Six-Dimensional Quantum Mechanical Study on a New Potential Energy Surface Based on the RPBE Functional. *J. Chem. Phys.* **2017**, *146*, 164706, DOI: 10.1063/1.4982051.

(46) Liu, Q.; Zhou, X.; Zhou, L.; Zhang, Y.; Luo, X.; Guo, H.; Jiang, B. Constructing High-Dimensional Neural Network Potential Energy Surfaces for Gas–Surface Scattering and Reactions. *J. Phys. Chem. C* **2018**, *122*, 1761–1769, DOI: 10.1021/acs.jpcc.7b12064.

(47) Jiang, B.; Guo, H. Towards an Accurate Specific Reaction Parameter Density Functional for Water Dissociation on Ni(111): RPBE versus PW91. *Phys. Chem. Chem. Phys.* **2016**, *18*, 21817–21824, DOI: 10.1039/C6CP03707K.

(48) Campbell, V. L.; Chen, N.; Guo, H.; Jackson, B.; Utz, A. L. Substrate Vibrations as Promoters of Chemical Reactivity on Metal Surfaces. *J. Phys. Chem. A* **2015**, *119*, 12434–12441, DOI: 10.1021/acs.jpca.5b07873.

(49) Chadwick, H.; Migliorini, D.; Kroes, G. J. CHD_3 Dissociation on Pt(111): A Comparison of the Reaction Dynamics Based on the PBE Functional and on a Specific Reaction Parameter Functional. *J. Chem. Phys.* **2018**, *149*, 044701, DOI: 10.1063/1.5039458.

(50) Ludwig, J.; Vlachos, D. G. Ab Initio Molecular Dynamics of Hydrogen Dissociation on Metal Surfaces Using Neural Networks and Novelty Sampling. *J. Chem. Phys.* **2007**, *127*, 154716, DOI: 10.1063/1.2794338.

(51) Golibrzuch, K.; Bartels, N.; Auerbach, D. J.; Wodtke, A. M. The Dynamics of Molecular Interactions and Chemical Reactions at Metal Surfaces: Testing the Foundations of Theory. *Annu. Rev. Phys. Chem.* **2015**, *66*, 399–425, DOI: 10.1146/annurev-physchem-040214-121958.

(52) White, J. D.; Chen, J.; Matsiev, D.; Auerbach, D. J.; Wodtke, A. M. Conversion of Large-Amplitude Vibration to Electron Excitation at a Metal Surface. *Nature* **2005**, *433*, 503–505, DOI: 10.1038/nature03213.

(53) Nahler, N. H.; White, J. D.; LaRue, J.; Auerbach, D. J.; Wodtke, A. M. Inverse Velocity Dependence of Vibrationally Promoted Electron Emission from a Metal Surface. *Science* **2008**, *321*, 1191–1194, DOI: 10.1126/science.1160040.

(54) Bünermann, O.; Jiang, H.; Dorenkamp, Y.; Kandratsenka, A.; Janke, S.; Auerbach, D. J.; Wodtke, A. M. Electron-Hole Pair Excitation Determines the Mechanism of Hydrogen Atom Adsorption. *Science* **2015**, *350*, 1346–1349, DOI: 10.1126/science.aad4972.

(55) Jiang, B.; Alducin, M.; Guo, H. Electron–Hole Pair Effects in Polyatomic Dissociative Chemisorption: Water on Ni(111). *J. Phys. Chem. Lett.* **2016**, *7*, 327–331, DOI: 10.1021/acs.jpclett.5b02737.

(56) Foulkes, W. M. C.; Mitas, L.; Needs, R. J.; Rajagopal, G. Quantum Monte Carlo Simulations of Solids. *Rev. Mod. Phys.* **2001**, *73*, 33–83, DOI: 10.1103/RevModPhys.73.33.

(57) Doblhoff-Dier, K.; Meyer, J.; Hoggan, P. E.; Kroes, G.-J. Quantum Monte Carlo Calculations on a Benchmark Molecule–Metal Surface Reaction: H_2 + Cu(111). *J. Chem. Theory Comput.* **2017**, *13*, 3208–3219, DOI: 10.1021/acs.jctc.7b00344.

(58) Powell, A. D.; Kroes, G.-J.; Doblhoff-Dier, K. Quantum Monte Carlo Calculations on Dissociative Chemisorption of H_2 + Al(110): Minimum Barrier Heights and Their Comparison to DFT Values. *J. Chem. Phys.* **2020**, *153*, 224701, DOI: 10.1063/5.0022919.

(59) Pozzo, M.; Alfè, D. Hydrogen Dissociation on Mg(0001) Studied via Quantum Monte Carlo Calculations. *Phys. Rev. B* **2008**, *78*, 245313, DOI: 10.1103/PhysRevB.78.245313.

(60) Johnson III, R. D. Computational Chemistry Comparison and Benchmark Database, NIST Standard Reference Database 101, National Institute of Standards and Technology: 2020, DOI: 10.18434/T47C7Z.

(61) Ji, D.-P.; Zhu, Q.; Wang, S.-Q. Detailed First-Principles Studies on Surface Energy and Work Function of Hexagonal Metals. *Surf. Sci.* **2016**, *651*, 137–146, DOI: 10.1016/j.susc.2016.04.007.

(62) Garron, R. Photoelectricité - Rendement Photoelectriques Des Couches Minces de Magnesium. *C.R. Hebd. Seances Acad. Sci.* **1964**, *258*, 1458.

(63) Österlund, L.; Zorić, I.; Kasemo, B. Dissociative Sticking of O_2 on Al(111). *Phys. Rev. B* **1997**, *55*, 15452–15455, DOI: 10.1103/PhysRevB.55.15452.

(64) Yin, R.; Zhang, Y.; Libisch, F.; Carter, E. A.; Guo, H.; Jiang, B. Dissociative Chemisorption of O_2 on Al(111): Dynamics on a Correlated Wave-Function-Based Potential Energy Surface. *J. Phys. Chem. Lett.* **2018**, *9*, 3271–3277, DOI: 10.1021/acs.jpclett.8b01470.

(65) Kurahashi, M.; Yamauchi, Y. Steric Effect in O_2 Sticking on Al(111): Preference for Parallel Geometry. *Phys. Rev. Lett.* **2013**, *110*, 246102, DOI: 10.1103/PhysRevLett.110.246102.

(66) Katz, G.; Kosloff, R.; Zeiri, Y. Abstractive Dissociation of Oxygen over Al(111): A Nonadiabatic Quantum Model. *J. Chem. Phys.* **2004**, *120*, 3931–3948, DOI: 10.1063/1.1635360.

(67) Mosch, C.; Koukounas, C.; Bacalis, N.; Metropoulos, A.; Gross, A.; Mavridis, A. Interaction of Dioxygen with Al Clusters and Al(111): A Comparative Theoretical Study. *J. Phys. Chem. C* **2008**, *112*, 6924–6932, DOI: 10.1021/jp711991b.

(68) Livshits, E.; Baer, R.; Kosloff, R. Deleterious Effects of Long-Range Self-Repulsion on the Density Functional Description of O_2 Sticking on Aluminum. *J. Phys. Chem. A* **2009**, *113*, 7521–7527, DOI: 10.1021/jp900892r.

(69) Bacalis, N. C.; Metropoulos, A.; Gross, A. Theoretical Study of the O_2 Interaction with a Tetrahedral Al_4 Cluster. *J. Phys. Chem. A* **2010**, *114*, 11746–11750, DOI: 10.1021/jp1052198.

(70) Liu, H.-R.; Xiang, H.; Gong, X. G. First Principles Study of Adsorption of O_2 on Al Surface with Hybrid Functionals. *J. Chem. Phys.* **2011**, *135*, 214702, DOI: 10.1063/1.3665032.

(71) Cheng, J.; Libisch, F.; Carter, E. A. Dissociative Adsorption of O_2 on Al(111): The Role of Orientational Degrees of Freedom. *J. Phys. Chem. Lett.* **2015**, *6*, 1661–1665, DOI: 10.1021/acs.jpclett.5b00597.

(72) Paranthaman, S.; Moon, J.; Hong, K.; Kim, J.; Kim, D. E.; Kim, J.; Kim, T. K. Reactivity of Molecular Oxygen with Aluminum Clusters: Density Functional and Ab Initio Molecular Dynamics Simulation Study. *Int. J. Quantum Chem.* **2016**, *116*, 547–554, DOI: 10.1002/qua.25080.

(73) Martin-Gondre, L.; Crespos, C.; Larrégaray, P.; Rayez, J. C.; Conte, D.; van Ootegem, B. Detailed Description of the Flexible Periodic London–Eyring–Polanyi–Sato Potential Energy Function. *Chem. Phys.* **2010**, *367*, 136–147, DOI: 10.1016/j.chemphys.2009.11.012.

(74) Karplus, M.; Porter, R. N.; Sharma, R. D. Exchange Reactions with Activation Energy. I. Simple Barrier Potential for (H, H_2). *J. Chem. Phys.* **1965**, *43*, 3259–3287, DOI: 10.1063/1.1697301.

(75) Smeets, E. W.; Voss, J.; Kroes, G.-J. Specific Reaction Parameter Density Functional Based on the Meta-Generalized Gradient Approximation: Application to H_2 + Cu(111) and H_2 + Ag(111). *J. Phys. Chem. A* **2019**, *123*, 5395–5406, DOI: 10.1021/acs.jpca.9b02914.

(76) Heyd, J.; Scuseria, G. E.; Ernzerhof, M. Hybrid Functionals Based on a Screened Coulomb Potential. *J. Chem. Phys.* **2003**, *118*, 8207–8215, DOI: 10.1063/1.1564060.

(77) Heyd, J.; Scuseria, G. E.; Ernzerhof, M. Erratum: "Hybrid Functionals Based on a Screened Coulomb Potential" [J. Chem. Phys. 118, 8207 (2003)]. *J. Chem. Phys.* **2006**, *124*, 219906, DOI: 10.1063/1.2204597.

(78) Sun, J.; Xiao, B.; Fang, Y.; Haunschild, R.; Hao, P.; Ruzsinszky, A.; Csonka, G. I.; Scuseria, G. E.; Perdew, J. P. Density Functionals That Recognize Covalent, Metallic, and Weak Bonds. *Phys. Rev. Lett.* **2013**, *111*, 106401, DOI: 10.1103/PhysRevLett.111.106401.

(79) Cortona, P. Note: Theoretical Mixing Coefficients for Hybrid Functionals. *J. Chem. Phys.* **2012**, *136*, 086101, DOI: 10.1063/1.3690462.

(80) Guido, C. A.; Brémond, E.; Adamo, C.; Cortona, P. Communication: One Third: A New Recipe for the PBE0 Paradigm. *J. Chem. Phys.* **2013**, *138*, 021104, DOI: 10.1063/1.4775591.

(81) Truong, T. N.; Duncan, W. A New Direct Ab Initio Dynamics Method for Calculating Thermal Rate Constants from Density Functional Theory. *J. Chem. Phys.* **1994**, *101*, 7408–7414, DOI: 10.1063/1.468299.

(82) Lynch, B. J.; Fast, P. L.; Harris, M.; Truhlar, D. G. Adiabatic Connection for Kinetics. *J. Phys. Chem. A* **2000**, *104*, 4811–4815, DOI: 10.1021/jp000497z.

(83) Zhao, Y.; Truhlar, D. G. Exploring the Limit of Accuracy of the Global Hybrid Meta Density Functional for Main-Group Thermochemistry, Kinetics, and Noncovalent Interactions. *J. Chem. Theory Comput.* **2008**, *4*, 1849–1868, DOI: 10.1021/ct800246v.

(84) Zhao, Y.; Truhlar, D. G. Density Functional Theory for Reaction Energies: Test of Meta and Hybrid Meta Functionals, Range-Separated Functionals, and Other High-Performance Functionals. *J. Chem. Theory Comput.* **2011**, *7*, 669–676, DOI: 10.1021/ct1006604.

(85) Brémond, É.; Pérez-Jiménez, Á. J.; Sancho-García, J. C.; Adamo, C. Range-Separated Hybrid Density Functionals Made Simple. *J. Chem. Phys.* **2019**, *150*, 201102, DOI: 10.1063/1.5097164.

(86) Moltved, K. A.; Kepp, K. P. The Metal Hydride Problem of Computational Chemistry: Origins and Consequences. *J. Phys. Chem. A* **2019**, *123*, 2888–2900, DOI: 10.1021/acs.jpca.9b02367.

(87) Zhao, Q.; Kulik, H. J. Stable Surfaces That Bind Too Tightly: Can Range-Separated Hybrids or DFT+U Improve Paradoxical Descriptions of Surface Chemistry? *J. Phys. Chem. Lett.* **2019**, *10*, 5090–5098, DOI: 10.1021/acs.jpclett.9b01650.

(88) Laikov, D. N. Simple Exchange Hole Models for Long-Range-Corrected Density Functionals. *J. Chem. Phys.* **2019**, *151*, 094106, DOI: 10.1063/1.5110633.

(89) Jana, S.; Patra, A.; Constantin, L. A.; Samal, P. Screened Range-Separated Hybrid by Balancing the Compact and Slowly Varying Density Regimes: Satisfaction of Local Density Linear Response. *J. Chem. Phys.* **2020**, *152*, 044111, DOI: 10.1063/1.5131530.

(90) Kresse, G.; Hafner, J. Ab Initio Molecular-Dynamics Simulation of the Liquid-Metal–Amorphous-Semiconductor Transition in Germanium. *Phys. Rev. B* **1994**, *49*, 14251–14269, DOI: 10.1103/PhysRevB.49.14251.

(91) Kresse, G.; Hafner, J. Ab Initio Molecular Dynamics for Liquid Metals. *Phys. Rev. B* **1993**, *47*, 558–561, DOI: 10.1103/PhysRevB.47.558.

(92) Kresse, G.; Furthmüller, J. Efficient Iterative Schemes for Ab Initio Total-Energy Calculations Using a Plane-Wave Basis Set. *Phys. Rev. B* **1996**, *54*, 11169–11186, DOI: 10.1103/PhysRevB.54.11169.

(93) Kresse, G.; Furthmüller, J. Efficiency of Ab-Initio Total Energy Calculations for Metals and Semiconductors Using a Plane-Wave Basis Set. *Comput. Mater. Sci.* **1996**, *6*, 15–50, DOI: 10.1016/0927-0256(96)00008-0.

(94) Kresse, G.; Joubert, D. From Ultrasoft Pseudopotentials to the Projector Augmented-Wave Method. *Phys. Rev. B* **1999**, *59*, 1758–1775, DOI: 10.1103/PhysRevB.59.1758.

(95) Blöchl, P. E. Projector Augmented-Wave Method. *Phys. Rev. B* **1994**, *50*, 17953–17979, DOI: 10.1103/PhysRevB.50.17953.

(96) Methfessel, M.; Paxton, A. T. High-Precision Sampling for Brillouin-Zone Integration in Metals. *Phys. Rev. B* **1989**, *40*, 3616–3621, DOI: 10.1103/PhysRevB.40.3616.

(97) Haas, P.; Tran, F.; Blaha, P. Calculation of the Lattice Constant of Solids with Semilocal Functionals. *Phys. Rev. B* **2009**, *79*, 085104, DOI: 10.1103/PhysRevB.79.085104.

(98) Jona, F.; Sondericker, D.; Marcus, P. M. Al(111) Revisited. *J. Phys. C: Solid State Phys.* **1980**, *13*, L155–L158, DOI: 10.1088/0022-3719/13/8/004.

(99) Busnengo, H. F.; Salin, A.; Dong, W. Representation of the 6D Potential Energy Surface for a Diatomic Molecule near a Solid Surface. *J. Chem. Phys.* **2000**, *112*, 7641–7651, DOI: 10.1063/1.481377.

(100) Porter, R. N.; Raff, L. M. In *Dynamics of Molecular Collisions: Part B*, Miller, W. H., Ed.; Modern Theoretical Chemistry; Springer US: Boston, MA, 1976, pp 1–52, DOI: 10.1007/978-1-4757-0644-4_1.

(101) Brink, D.; Satchler, G., *Angular Momentum*, 2nd ed.; Oxford University Press: 1968; 87 pp.

(102) Bulirsch, R.; Stoer, J. Numerical Treatment of Ordinary Differential Equations by Extrapolation Methods. *Numer. Math.* **1966**, *8*, 1–13, DOI: 10.1007/BF02165234.

(103) Stoer, J.; Bulirsch, R. In *Introduction to Numerical Analysis*, Stoer, J., Bulirsch, R., Eds.; Springer: New York, NY, 1980, pp 244–313, DOI: 10.1007/978-1-4757-5592-3_5.

(104) Nattino, F.; Ueta, H.; Chadwick, H.; van Reijzen, M. E.; Beck, R. D.; Jackson, B.; van Hemert, M. C.; Kroes, G.-J. Ab Initio Molecular Dynamics Calculations versus Quantum-State-Resolved Experiments on CHD_3 + Pt(111): New Insights into a Prototypical Gas–Surface Reaction. *J. Phys. Chem. Lett.* **2014**, *5*, 1294–1299, DOI: 10.1021/jz500233n.

(105) Karikorpi, M.; Holloway, S.; Henriksen, N.; Nørskov, J. K. Dynamics of Molecule-Surface Interactions. *Surf. Sci.* **1987**, *179*, L41–L48, DOI: 10.1016/0039-6028(87)90111-7.

(106) Binetti, M.; Weiße, O.; Hasselbrink, E.; Katz, G.; Kosloff, R.; Zeiri, Y. The Role of Nonadiabatic Pathways and Molecular Rotations in the Oxygen Abstraction Reaction on the Al(111) Surface. *Chem. Phys. Lett.* **2003**, *373*, 366–371, DOI: 10.1016/S0009-2614(03)00586-4.

(107) Tiwari, A. K.; Nave, S.; Jackson, B. The Temperature Dependence of Methane Dissociation on Ni(111) and Pt(111): Mixed Quantum-Classical Studies of the Lattice Response. *J. Chem. Phys.* **2010**, *132*, 134702, DOI: 10.1063/1.3357415.

(108) Tiwari, A. K.; Nave, S.; Jackson, B. Methane Dissociation on Ni(111): A New Understanding of the Lattice Effect. *Phys. Rev. Lett.* **2009**, *103*, 253201, DOI: 10.1103/PhysRevLett.103.253201.

(109) Mori-Sánchez, P.; Cohen, A. J.; Yang, W. Many-Electron Self-Interaction Error in Approximate Density Functionals. *J. Chem. Phys.* **2006**, *125*, 201102, DOI: 10.1063/1.2403848.

(110) Mori-Sánchez, P.; Cohen, A. J.; Yang, W. Localization and Delocalization Errors in Density Functional Theory and Implications for Band-Gap Prediction. *Phys. Rev. Lett.* **2008**, *100*, 146401, DOI: 10.1103/PhysRevLett.100.146401.

(111) Bao, J. L.; Gagliardi, L.; Truhlar, D. G. Self-Interaction Error in Density Functional Theory: An Appraisal. *J. Phys. Chem. Lett.* **2018**, *9*, 2353–2358, DOI: 10.1021/acs.jpclett.8b00242.

(112) Bartlett, R. J. Adventures in DFT by a Wavefunction Theorist. *J. Chem. Phys.* **2019**, *151*, 160901, DOI: 10.1063/1.5116338.

(113) Berland, K.; Jiao, Y.; Lee, J.-H.; Rangel, T.; Neaton, J. B.; Hyldgaard, P. Assessment of Two Hybrid van Der Waals Density Functionals for Covalent and Non-Covalent Binding of Molecules. *J. Chem. Phys.* **2017**, *146*, 234106, DOI: 10.1063/1.4986522.

(114) Jiao, Y.; Schröder, E.; Hyldgaard, P. Extent of Fock-Exchange Mixing for a Hybrid van Der Waals Density Functional? *J. Chem. Phys.* **2018**, *148*, 194115, DOI: 10.1063/1.5012870.

(115) Marom, N.; Tkatchenko, A.; Rossi, M.; Gobre, V. V.; Hod, O.; Scheffler, M.; Kronik, L. Dispersion Interactions with Density-Functional Theory: Benchmarking Semiempirical and Interatomic Pairwise Corrected Density Functionals. *J. Chem. Theory Comput.* **2011**, *7*, 3944–3951, DOI: 10.1021/ct2005616.

(116) Lonsdale, D. R.; Goerigk, L. The One-Electron Self-Interaction Error in 74 Density Functional Approximations: A Case Study on Hydrogenic Mono- and Dinuclear Systems. *Phys. Chem. Chem. Phys.* **2020**, *22*, 15805–15830, DOI: 10.1039/D0CP01275K.

(117) Kim, M.-C.; Sim, E.; Burke, K. Understanding and Reducing Errors in Density Functional Calculations. *Phys. Rev. Lett.* **2013**, *111*, 073003, DOI: 10.1103/PhysRevLett.111.073003.

(118) Vuckovic, S.; Song, S.; Kozlowski, J.; Sim, E.; Burke, K. Density Functional Analysis: The Theory of Density-Corrected DFT. *J. Chem. Theory Comput.* **2019**, *15*, 6636–6646, DOI: 10.1021/acs.jctc.9b00826.

(119) Song, S.; Sim, E.; Vuckovic, S.; Burke, K. How Errors in Densities Contaminate Empirical Density Functionals http://arxiv.org/abs/2008.01261 (accessed 10/28/2020).

(120) Skelton, J. M.; Gunn, D. S. D.; Metz, S.; Parker, S. C. Accuracy of Hybrid Functionals with Non-Self-Consistent Kohn–Sham Orbitals for Predicting the Properties of Semiconductors. *J. Chem. Theory Comput.* **2020**, *16*, 3543–3557, DOI: 10.1021/acs.jctc.9b01218.

(121) Patra, A.; Peng, H.; Sun, J.; Perdew, J. P. Rethinking CO Adsorption on Transition-Metal Surfaces: Effect of Density-Driven Self-Interaction Errors. *Phys. Rev. B* **2019**, *100*, 035442, DOI: 10.1103/PhysRevB.100.035442.

(122) Krukau, A. V.; Vydrov, O. A.; Izmaylov, A. F.; Scuseria, G. E. Influence of the Exchange Screening Parameter on the Performance of Screened Hybrid Functionals. *J. Chem. Phys.* **2006**, *125*, 224106, DOI: 10.1063/1.2404663.

(123) Perdew, J. P.; Ruzsinszky, A.; Tao, J.; Staroverov, V. N.; Scuseria, G. E.; Csonka, G. I. Prescription for the Design and Selection of Density Functional Approximations: More Constraint Satisfaction with Fewer Fits. *J. Chem. Phys.* **2005**, *123*, 062201, DOI: 10.1063/1.1904565.

(124) Dion, M.; Rydberg, H.; Schröder, E.; Langreth, D. C.; Lundqvist, B. I. Van Der Waals Density Functional for General Geometries. *Phys. Rev. Lett.* **2004**, *92*, 246401, DOI: 10.1103/PhysRevLett.92.246401.

(125) Perdew, J. P.; Ernzerhof, M.; Burke, K. Rationale for Mixing Exact Exchange with Density Functional Approximations. *J. Chem. Phys.* **1996**, *105*, 9982–9985, DOI: 10.1063/1.472933.

(126) Adamo, C.; Barone, V. Toward Reliable Density Functional Methods without Adjustable Parameters: The PBE0 Model. *J. Chem. Phys.* **1999**, *110*, 6158–6170, DOI: 10.1063/1.478522.

(127) Cohen, A. J.; Mori-Sánchez, P.; Yang, W. Challenges for Density Functional Theory. *Chem. Rev.* **2012**, *112*, 289–320, DOI: 10.1021/cr200107z.

(128) Derry, G. N.; Kern, M. E.; Worth, E. H. Recommended Values of Clean Metal Surface Work Functions. *J. Vac. Sci. Technol. A* **2015**, *33*, 060801, DOI: 10.1116/1.4934685.

(129) Ramírez-Solís, A.; Vigué, J.; Hinojosa, G.; Saint-Martin, H. Solving the CH_4^- Riddle: The Fundamental Role of Spin to Explain Metastable Anionic Methane. *Phys. Rev. Lett.* **2020**, *124*, 056001, DOI: 10.1103/PhysRevLett.124.056001.

(130) Kohn, W.; Sham, L. J. Self-Consistent Equations Including Exchange and Correlation Effects. *Phys. Rev.* **1965**, *140*, A1133–A1138, DOI: 10.1103/PhysRev.140.A1133.

(131) Perdew, J. P.; Wang, Y. Accurate and Simple Analytic Representation of the Electron-Gas Correlation Energy. *Phys. Rev. B* **1992**, *45*, 13244–13249, DOI: 10.1103/PhysRevB.45.13244.

(132) Perdew, J. P.; Ruzsinszky, A.; Csonka, G. I.; Vydrov, O. A.; Scuseria, G. E.; Constantin, L. A.; Zhou, X.; Burke, K. Restoring the Density-Gradient Expansion for Exchange in Solids and Surfaces. *Phys. Rev. Lett.* **2008**, *100*, 136406, DOI: 10.1103/PhysRevLett.100.136406.

(133) Sun, J.; Ruzsinszky, A.; Perdew, J. P. Strongly Constrained and Appropriately Normed Semilocal Density Functional. *Phys. Rev. Lett.* **2015**, *115*, 036402, DOI: 10.1103/PhysRevLett.115.036402.

(134) Peng, H.; Yang, Z.-H.; Perdew, J. P.; Sun, J. Versatile van Der Waals Density Functional Based on a Meta-Generalized Gradient Approximation. *Phys. Rev. X* **2016**, *6*, 041005, DOI: 10.1103/PhysRevX.6.041005.

(135) Tran, R.; Li, X.-G.; Montoya, J. H.; Winston, D.; Persson, K. A.; Ong, S. P. Anisotropic Work Function of Elemental Crystals. *Surf. Sci.* **2019**, *687*, 48–55, DOI: 10.1016/j.susc.2019.05.002.

(136) Richard, R. M.; Marshall, M. S.; Dolgounitcheva, O.; Ortiz, J. V.; Brédas, J.-L.; Marom, N.; Sherrill, C. D. Accurate Ionization Potentials and Electron Affinities of Acceptor Molecules I. Reference Data at the CCSD(T) Complete Basis Set Limit. *J. Chem. Theory Comput.* **2016**, *12*, 595–604, DOI: 10.1021/acs.jctc.5b00875.

(137) Goerigk, L.; Grimme, S. A General Database for Main Group Thermochemistry, Kinetics, and Noncovalent Interactions - Assessment of Common and Reparameterized (Meta-)GGA Density Functionals. *J. Chem. Theory Comput.* **2010**, *6*, 107–126, DOI: 10.1021/ct900489g.

(138) Su, N. Q.; Xu, X. Insights into Direct Methods for Predictions of Ionization Potential and Electron Affinity in Density Functional Theory. *J. Phys. Chem. Lett.* **2019**, *10*, 2692–2699, DOI: 10.1021/acs.jpclett.9b01052.

(139) Feibelman, P. J. Energetics of Steps on Pt(111). *Phys. Rev. B* **1995**, *52*, 16845–16854, DOI: 10.1103/PhysRevB.52.16845.

(140) Brémond, É.; Pérez-Jiménez, Á. J.; Sancho-García, J. C.; Adamo, C. Range-Separated Hybrid and Double-Hybrid Density Functionals: A Quest for the Determination of the Range-Separation Parameter. *J. Chem. Phys.* **2020**, *152*, 244124, DOI: 10.1063/5.0010976.

(141) Migliorini, D.; Nattino, F.; Tiwari, A. K.; Kroes, G.-J. HOD on Ni(111): Ab Initio Molecular Dynamics Prediction of Molecular Beam Experiments. *J. Chem. Phys.* **2018**, *149*, 244706, DOI: 10.1063/1.5059357.

(142) Nattino, F.; Díaz, C.; Jackson, B.; Kroes, G.-J. Effect of Surface Motion on the Rotational Quadrupole Alignment Parameter of D_2 Reacting on Cu(111). *Phys. Rev. Lett.* **2012**, *108*, 236104, DOI: 10.1103/PhysRevLett.108.236104.

(143) Ghassemi, E. N.; Somers, M. F.; Kroes, G.-J. Assessment of Two Problems of Specific Reaction Parameter Density Functional Theory: Sticking and Diffraction of H_2 on Pt(111). *J. Phys. Chem. C* **2019**, *123*, 10406–10418, DOI: 10.1021/acs.jpcc.9b00981.

(144) Gerrits, N.; Geweke, J.; Smeets, E. W. F.; Voss, J.; Wodtke, A. M.; Kroes, G.-J. Closing the Gap Between Experiment and Theory: Reactive Scattering of HCl from Au(111). *J. Phys. Chem. C* **2020**, *124*, 15944–15960, DOI: 10.1021/acs.jpcc.0c03756.

(145) Kuebler, N. A.; Robin, M. B.; Yang, J. J.; Gedanken, A.; Herrick, D. R. Fully Resolved Zeeman Pattern in the Stern-Gerlach Deflection Spectrum of O_2 ($^3\Sigma_g^-, K = 1$). *Phys. Rev. A* **1988**, *38*, 737–749, DOI: 10.1103/PhysRevA.38.737.

(146) Rettner, C. T.; DeLouise, L. A.; Auerbach, D. J. Effect of Incidence Kinetic Energy and Surface Coverage on the Dissociative Chemisorption of Oxygen on W(110). *J. Chem. Phys.* **1986**, *85*, 1131–1149, DOI: 10.1063/1.451310.

(147) Montemore, M. M.; van Spronsen, M. A.; Madix, R. J.; Friend, C. M. O_2 Activation by Metal Surfaces: Implications for Bonding and Reactivity on Heterogeneous Catalysts. *Chem. Rev.* **2018**, *118*, 2816–2862, DOI: 10.1021/acs.chemrev.7b00217.

(148) Eichler, A.; Hafner, J. Molecular Precursors in the Dissociative Adsorption of O_2 on Pt(111). *Phys. Rev. Lett.* **1997**, *79*, 4481–4484, DOI: 10.1103/PhysRevLett.79.4481.

(149) Eichler, A.; Mittendorfer, F.; Hafner, J. Precursor-Mediated Adsorption of Oxygen on the (111) Surfaces of Platinum-Group Metals. *Phys. Rev. B* **2000**, *62*, 4744–4755, DOI: 10.1103/PhysRevB.62.4744.

(150) Sendner, C.; Groß, A. Kinetic Monte Carlo Simulations of the Interaction of Oxygen with Pt(111). *J. Chem. Phys.* **2007**, *127*, 014704, DOI: 10.1063/1.2748379.

(151) Zhou, Y.; Zhou, L.; Hu, X.; Xie, D. Dynamics Studies of O_2 Collision on Pt(111) Using a Global Potential Energy Surface. *J. Phys. Chem. C* **2020**, *124*, 10573–10583, DOI: 10.1021/acs.jpcc.0c01247.

(152) Lončarić, I.; Alducin, M.; Juaristi, J. I.; Novko, D. CO Stretch Vibration Lives Long on Au(111). *J. Phys. Chem. Lett.* **2019**, *10*, 1043–1047, DOI: 10.1021/acs.jpclett.9b00069.

(153) Lee, K.; Murray, É. D.; Kong, L.; Lundqvist, B. I.; Langreth, D. C. Higher-Accuracy van Der Waals Density Functional. *Phys. Rev. B* **2010**, *82*, 081101(R), DOI: 10.1103/PhysRevB.82.081101.

(154) Sun, J.; Haunschild, R.; Xiao, B.; Bulik, I. W.; Scuseria, G. E.; Perdew, J. P. Semilocal and Hybrid Meta-Generalized Gradient Approximations Based on the Understanding of the Kinetic-Energy-Density Dependence. *J. Chem. Phys.* **2013**, *138*, 044113, DOI: 10.1063/1.4789414.

(155) Baer, R.; Livshits, E.; Salzner, U. Tuned Range-Separated Hybrids in Density Functional Theory. *Annu. Rev. Phys. Chem.* **2010**, *61*, 85–109, DOI: 10.1146/annurev.physchem.012809.103321.

(156) Refaely-Abramson, S.; Sharifzadeh, S.; Govind, N.; Autschbach, J.; Neaton, J. B.; Baer, R.; Kronik, L. Quasiparticle Spectra from a Nonempirical Optimally Tuned Range-Separated Hybrid Density Functional. *Phys. Rev. Lett.* **2012**, *109*, 226405, DOI: 10.1103/PhysRevLett.109.226405.

(157) Karolewski, A.; Kronik, L.; Kümmel, S. Using Optimally Tuned Range Separated Hybrid Functionals in Ground-State Calculations: Consequences and Caveats. *J. Chem. Phys.* **2013**, *138*, 204115, DOI: 10.1063/1.4807325.

(158) Tamblyn, I.; Refaely-Abramson, S.; Neaton, J. B.; Kronik, L. Simultaneous Determination of Structures, Vibrations, and Frontier Orbital Energies from a Self-Consistent Range-Separated Hybrid Functional. *J. Phys. Chem. Lett.* **2014**, *5*, 2734–2741, DOI: 10.1021/jz5010939.